Taylor & Francis
Taylor & Francis Group

ORIGINAL ARTICLE

⊕ OPEN ACCESS | Check for updates

Novel oxindole/benzofuran hybrids as potential dual CDK2/GSK-3β inhibitors targeting breast cancer: design, synthesis, biological evaluation, and *in silico* studies

Wagdy M. Eldehna[a], Sara T. Al-Rashood[b], Tarfah Al-Warhi[c], Razan O. Eskandrani[b], Amal Alharbi[b] and Ahmed M. El Kerdawy[d,e]

[a]Department of Pharmaceutical Chemistry, Faculty of Pharmacy, Kafrelsheikh University, Kafr El-Sheikh, Egypt; [b]Department of Pharmaceutical Chemistry, College of Pharmacy, King Saud University, Riyadh, Saudi Arabia; [c]Department of Chemistry, College of Science, Princess Nourah Bint Abdulrahman University, Riyadh, Saudi Arabia; [d]Department of Pharmaceutical Chemistry, Faculty of Pharmacy, Cairo University, Cairo, Egypt; [e]Department of Pharmaceutical Chemistry, Faculty of Pharmacy, New Giza University, Cairo, Egypt

ABSTRACT

The serine/threonine protein kinases CDK2 and GSK-3β are key oncotargets in breast cancer cell lines, therefore, in the present study three series of oxindole-benzofuran hybrids were designed and synthesised as dual CDK2/GSK-3β inhibitors targeting breast cancer (**5a–g**, **7a–h**, and **13a–b**). The N^1-unsubstituted oxindole derivatives, **series 5**, showed moderate to potent activity on both MCF-7 and T-47D breast cancer cell lines. Compounds **5d–f** showed the most potent cytotoxic activity with IC_{50} of 3.41, 3.45 and 2.27 μM, respectively, on MCF-7 and of 3.82, 4.53 and 7.80 μM, respectively, on T-47D cell lines, in comparison to the used reference standard (staurosporine) IC_{50} of 4.81 and 4.34 μM, respectively. On the other hand, the N^1-substituted oxindole derivatives, **series 7** and **13**, showed moderate to weak cytotoxic activity on both breast cancer cell lines. CDK2 and GSK-3β enzyme inhibition assay of **series 5** revealed that compounds **5d** and **5f** are showing potent dual CDK2/GSK-3β inhibitory activity with IC_{50} of 37.77 and 52.75 nM, respectively, on CDK2 and 32.09 and 40.13 nM, respectively, on GSK-3β. The most potent compounds **5d–f** caused cell cycle arrest in the G2/M phase in MCF-7 cells inducing cell apoptosis because of the CDK2/GSK-3β inhibition. Molecular docking studies showed that the newly synthesised N^1-unsubstituted oxindole hybrids have comparable binding patterns in both CDK2 and GSK-3β. The oxindole ring is accommodated in the hinge region interacting through hydrogen bonding with the backbone CO and NH of the key amino acids Glu81 and Leu83, respectively, in CDK2 and Asp133 and Val135, respectively, in GSK-3β. Whereas, in series **7** and **13**, the N^1-substitutions on the oxindole nucleus hinder the compounds from achieving these key interactions with hinge region amino acids what rationalises their moderate to low anti-proliferative activity.

1. Introduction

Protein kinases (PKs) represent the fifth largest human protein family comprising 518 proteins[1–2]. They are key regulators of cell functions through cellular signalling modulation and complex biological functions coordination such as cell growth, differentiation, proliferation, metabolism, migration, and apoptosis (programmed cell death)[1,3–5]. PKs exert their functions through catalysing the transfer of the gamma-phosphate group of an ATP molecule onto a substrate protein hydroxyl group (substrate protein phosphorylation) accomplishing cellular signals transduction and amplification[1]. According to the phosphorylated residue in the substrate protein, PKs are classified into tyrosine kinases (90 kinases) and serine/threonine kinases (385 kinases), with a small group of dual specificity kinases including MEK1 and MEK2 which could catalyse the phosphorylation of both tyrosine and threonine on target proteins[6–7].

The prominent and critical importance of PKs dictates strict regulation of their cellular levels and activities, therefore, PKs

dysregulation contributes to several diseases such as cancer, metabolic disorders (such as diabetes), cardiovascular diseases, neurodegenerative diseases (such as Alzheimer's disease), inflammatory disorders and autoimmune diseases (such as rheumatoid arthritis)[8]. The usage of PKs inhibitors is a promising strategy to manage their dysregulation in these diseases[8–11]. In cancer treatment, PK inhibitors represent a key class of targeted chemotherapy which is devoid of the common side effects of conventional cancer chemotherapy because they target cancer cells' signalling pathways and microenvironment with minimum undesirable effects on normal cells[12–15].

Breast cancer is a very common cancer type all over the world, and despite of its possible early detection by advanced diagnostic techniques, breast cancer is still considered the leading cause of death among women worldwide[16–17]. Thus, there is a serious continuous demand for the discovery of more effective anti-breast cancer agents. Several studies reported the overexpression of several PKs in primary as well as in metastatic breast cancers such as

---

vascular endothelial growth factor receptor (VEGFR)[18–20], fibroblast growth factor receptor (FGFR)[20–21], platelet-derived growth factor receptor (PDGFR)[20,22], cyclin dependent kinases (CDKs) and their activating cyclins[23–27], and glycogen synthase kinase 3β (GSK-3β)[28–30] and references therein.

CDKs, a family of serine/threonine protein kinases, are involved in several cellular functions such as division, proliferation, apoptosis, and gene transcription. CDK1, CDK2, CDK4 and CDK6 subtypes are responsible for the regulation of cell-cycle progression in its different phases, moreover, they play a pivotal role in cancer cell continuous proliferation[31–33]. CDK2 subtype, specifically, received a great attention as a therapeutic target for cancer treatment due to its key role in several cellular processes upon complexation with its activating cognate, cyclin A or E, in addition, dysregulation of CDK2 or its cyclin partners was detected in various cancers such as ovarian, lung, pancreatic carcinomas, melanoma as well as breast cancer [23–27,34–37]. The impact of CDK2 inhibition on cancer cells confirmed the validity of CDK2 as a promising anticancer drug target, therefore, many CDK2 inhibitors have been progressed through clinical trials (Figure 1)[34,35,38]. In particular, CDK2 inhibition was found to effectively hinder breast cancer cells proliferation including those resistant to hormonal therapy[39–41].

GSK-3, another serine/threonine protein kinase and an essential element of the WNT signalling pathway, contributes to several physiological processes ranging from gene expression to glycogen metabolism[42]. GSK-3 has two isozymes α and β encoded by two independent GSK-3 genes[43–48]. GSK-3β is known as the "multitasking kinase" due to its participation in several signalling pathways[49]. Dysregulated activity of GSK-3β is associated with several diseases such as type 2 diabetes, heart disease, chronic inflammatory diseases, neurodegenerative diseases, and cancer, therefore, GSK-3β inhibition is a potential approach for the treatment of these diseases[30,50]. GSK-3β is overexpressed in colon, pancreatic as well as breast cancers as it plays a key role in cancer cell proliferation and survival[28,29,51]. The overexpression of GSK-3β

correlates with poor prognosis in patients with breast cancer[28–29], moreover, aberrant nuclear accumulation of GSK-3β in five human breast cancer cell lines and in 70% of human breast carcinomas was reported[29], furthermore, GSK-3β inhibition suppressed the viability of breast cancer cells in vitro, moreover, GSK-3β inhibition overcomes chemoresistance in human breast cancer[52].

The complex nature of cancer mandates the implementation of multitarget treatment strategies[53–55]. Moreover, in several cancer types especially solid tumours, such as breast cancer, more than one PK is upregulated and contributes to carcinogenesis[54,56]. Furthermore, drug resistance is commonly developed by target PK mutation, target PK amplification/overexpression, or through upregulation of alternative/downstream pathways[54]. Thus, the use of multiple PK inhibitors is an emerging and appealing trend to overcome cancer development, progression, and resistance. A possible drawback of this approach is the pharmacokinetics (ADME) interference among the co-administered inhibitors, another concern is the potential toxicity of the used combination. To avoid these drawbacks, the design of small-molecules that are intentionally tailored to target more than one PK (multikinase inhibitors) was considered[53–55,57,58]. Multikinase inhibitors with favourable selectivity or multitarget selectivity (poly-specific inhibitors) might be more suitable for cancer treatment to balance efficacy and toxicity[53–55,57,58].

Dual CDKs/GSK-3β inhibition is a promising therapeutic approach to confront uncontrolled cancer cell proliferation[35,36,51,59–66]. In particular, CDK2 and GSK-3β share a high homologous sequence (33% amino acid identity) and are used as examples for the homological CMGC protein kinase family[59,64,67–75]. Therefore, designing dual CDK2/GSK-3β inhibitors as anticancer agents is an amenable and attractive strategy[65–66].

1H-indole-2,3-dione (isatin) is a privileged scaffold that emerged as a promising nucleus in medicinal chemistry demonstrating a broad range of pharmacological activities including antibacterial, anticonvulsant, antifungal, antiviral, as well as anticancer activity[76–78]. Isatin derivatives exert their anticancer activity
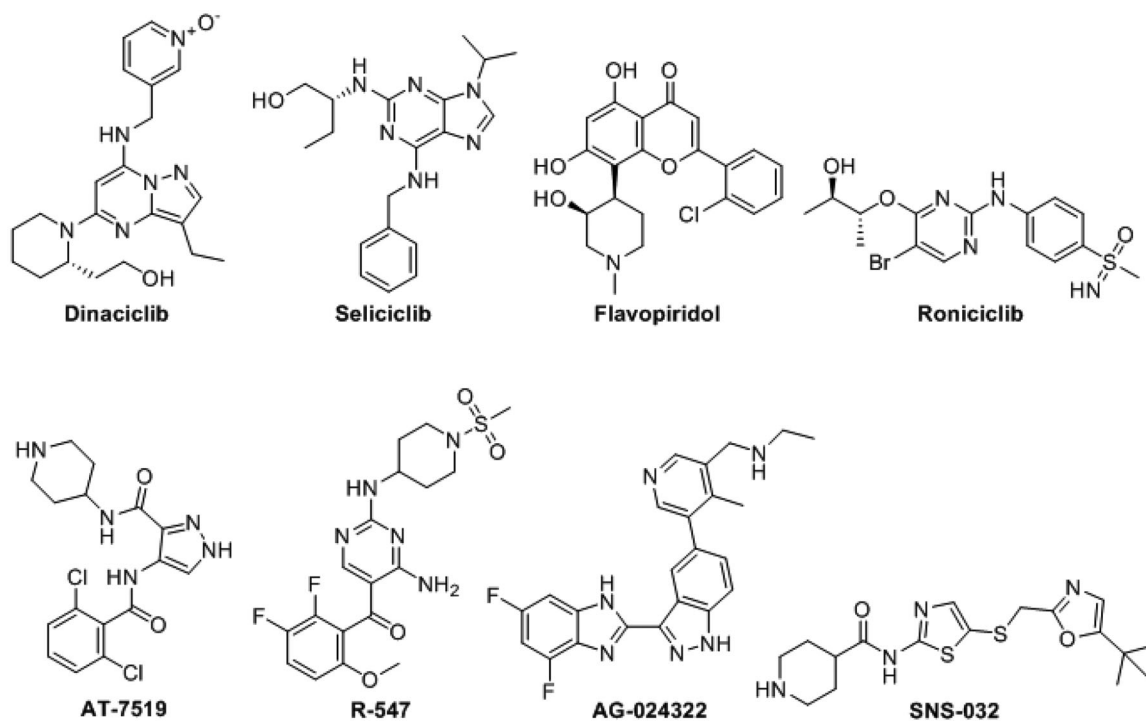

Figure 1. CDKs inhibitors in the clinical trial phases.

through several mechanisms such as inhibition and/or modulation of proteases, translation initiation, angiogenesis or tubulin polymerisation, moreover, PK inhibition is one of the key anticancer mechanisms of isatin derivatives[76–78]. Several oxindole-based multikinase inhibitors (Figure 2) have been approved for cancer treatment such as sunitinib (2006) for gastrointestinal stromal tumour and renal cell carcinoma as PDGFR and VEGFR inhibitor[79], and nintedanib (2014) for idiopathic pulmonary fibrosis as FGFR, PDGFR and VEGFR inhibitor[80]. Moreover, several oxindole derivatives have been designed and synthesised as inhibitors for diverse PKs such as FLT3 kinase[81], VEGFR[82–83], polo-like kinase 4 (PLK4)[84], aurora B kinase[85], p90 ribosomal S6 protein kinase 2 (RSK2)[86], microtubule affinity-regulating kinase 4 (MARK4)[87] as well as CDKs[78,88], and GSK-3β[59].

The naturally occurring oxindole derivative, indirubin, (Figure 2) has been identified as the main active ingredient of the traditional Chinese medicinal remedy, *Dang Gui Long Hui Wan* which is used to treat chronic myelocytic leukaemia (CML)[64,66,89]. Indirubin and its derivatives showed distinctive antiproliferative effect which is attributed to their inhibition of CDKs and GSK-3 through competing with ATP at the kinase domain[74,90–93].

Benzofuran is another privileged scaffold that demonstrated several desirable biological activities among which are analgesic, anti-inflammatory, antipyretic, antibacterial, antifungal, antiviral, antihyperglycemic, anti-hyperlipidemic, anti-oxidant, as well as anticancer activities[94–96]. Benzofuran derivatives mediate their anticancer activity through several mechanism such as farnesyltransferase, angiogenesis, oestrogen receptor, human peptide deformylase, tubulin polymerisation, and carbonic anhydrase inhibition[94,97] and reference therein. Moreover, some benzofuran derivatives exert their anticancer activity through PK inhibition such as Pim-1[98], mTOR signaling[99–100], Src kinase[101], as well as GSK-3β[51] (Figure 3).

Based on the reported PK inhibitory activity of isatin and benzofuran nuclei, specially, on the homologous CDK2 and GSK-3β kinases, a hybridisation strategy of these two privileged scaffolds was adapted to design dual CDK2/GSK-3β hybrid inhibitors which could target breast cancer. For the hybridisation strategy, the bioisosteric amido and uriedo moieties were used as linkers between the two nuclei, moreover, different substitution pattern and nature on the oxindole ring offering various electronic and lipophilic environments were introduced to study their impact on the activity (Figure 4). On account of the hydrophobic nature of the CDK2 binding site, it was anticipated that the grafting a hydrophobic substituent (such as Br) within the benzofuran motif could achieve a plenty of hydrophobic interactions.

The newly synthesised compounds were experimentally evaluated for their anti-proliferative activities against breast cancer cell lines T-47D and MCF-7. Compounds showed promising anti-proliferative activity were tested for their potential dual CDK2/GSK-3β inhibitory activity, moreover, compounds showed prominent anti-proliferative activity and *in vitro* PK inhibitory activity were investigated further by studying their effect on cell cycle progression and cell apoptosis. Furthermore, molecular docking studies were also performed to study the interaction of the newly synthesised hybrid compounds with CDK2 and GSK-3β kinase domain hot spots (key amino acids) to rationalise their biological activity and to reveal their probable binding mode.

2. Results and discussion

2.1. Chemistry

The synthetic strategies designed for the preparation of the target final compounds (**5a-g**, **7a-h** and **13a-b**) were illustrated in Schemes 1–3. In Scheme 1, bromobenzofuran-2-carbohydrazide **3** was prepared *via* reaction of ethylbromacetate with 5-bromosalicylaldehyde **1** in acetonitrile to furnish ethyl 5-bromobenzofuran-2-carboxylate **2**. Thereafter, the ester functionality was subjected to hydrazinolysis via refluxing hydrazine hydrate to afford the key intermediate hydrazide **3**, further; this key intermediate **3** was condensed with different isatin derivatives **4a-g** in absolute ethyl alcohol with catalytic drops of glacial acetic acid to get the final novel compounds **5a-g**.

In Scheme 2, isatin derivatives **4a** and **4d** were subjected to N-alkylation in anhydrous DMF to furnish N-substituted isatin **6a-h**,
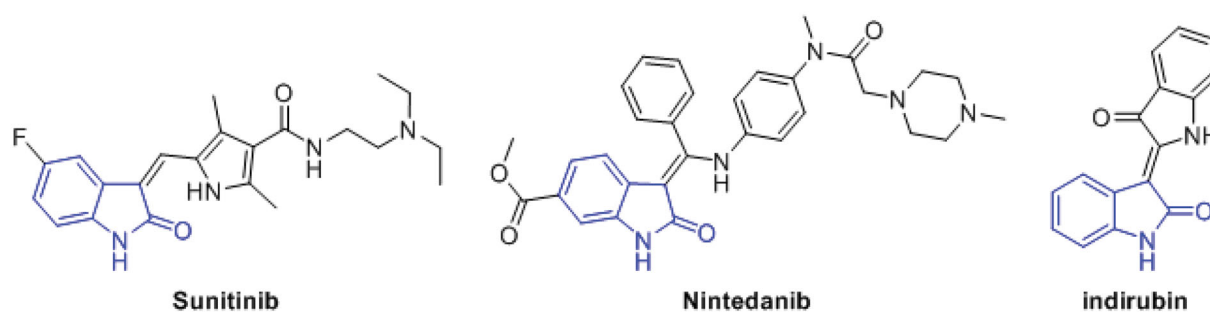

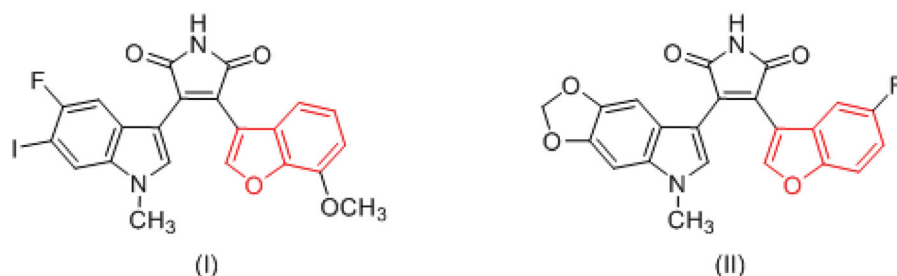**Figure 2.** Oxindole derivatives with multikinase activity.

Figure 3. Benzofuran derivatives with GSK-3β inhibitory activity.
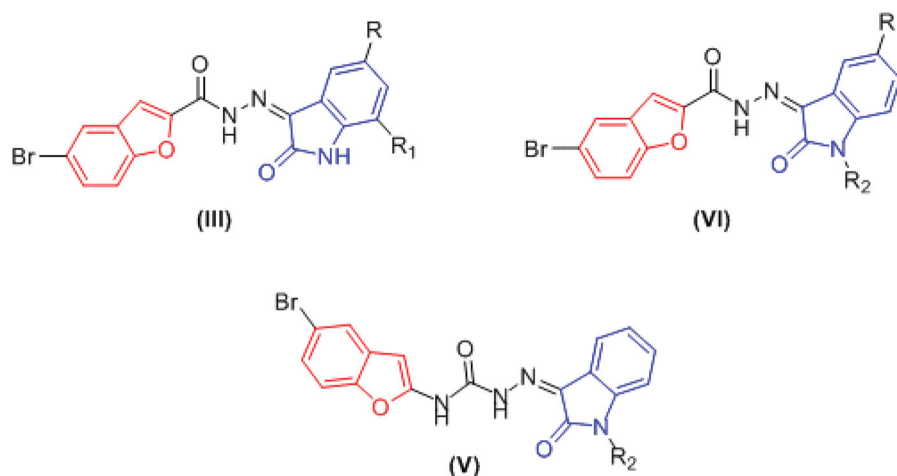
Figure 4. Designed oxindole/benzofuran dual CDK2/GSK-3β hybrid inhibitors.

4/5	R	R$_1$
a	H	H
b	F	H
c	Cl	H
d	Br	H
e	CH$_3$	H
f	OCH$_3$	H
g	CH$_3$	CH$_3$
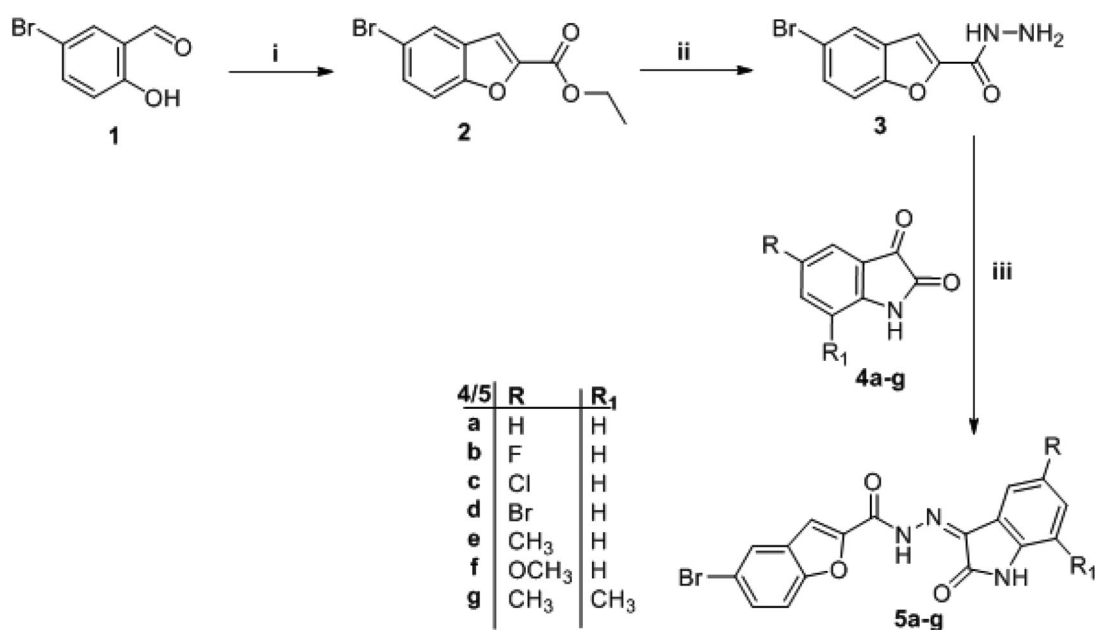
Scheme 1. Synthesis of target compounds **5a–g**; Reagents and conditions: (**i**) Ethyl bromoacetate/Acetonitrile/K$_2$CO$_3$/reflux 4 h, (**ii**) NH$_2$NH$_2$.H$_2$O/methanol/reflux 3 h, (**iii**) Ethanol/glacial acetic acid (Cat.)/reflux 4–7 h.

6/7	R	R$_2$
a	H	-CH$_3$
b	H	-CH$_2$CH=CH$_2$
c	H	-CH$_2$CH(CH$_3$)$_2$
d	H	-CH$_2$COOC$_2$H$_5$
e	H	-CH$_2$Ph
f	H	-CH$_2$CH$_2$Ph
g	Br	-CH$_2$CH(CH$_3$)$_2$
h	Br	-CH$_2$Ph
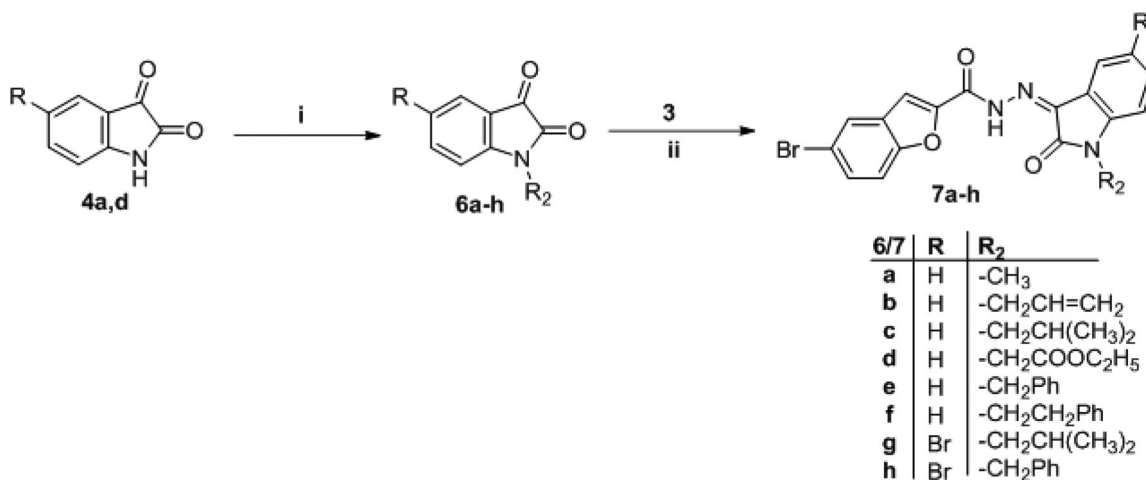
Scheme 2. Synthesis of target compounds **7a-h**; Reagents and conditions: (**i**) R$_2$-Br/anhydrous DMF/K$_2$CO$_3$/reflux 4 h, (**ii**) Ethanol/drops glacial acetic acid (Cat.)/reflux 4–7 h.
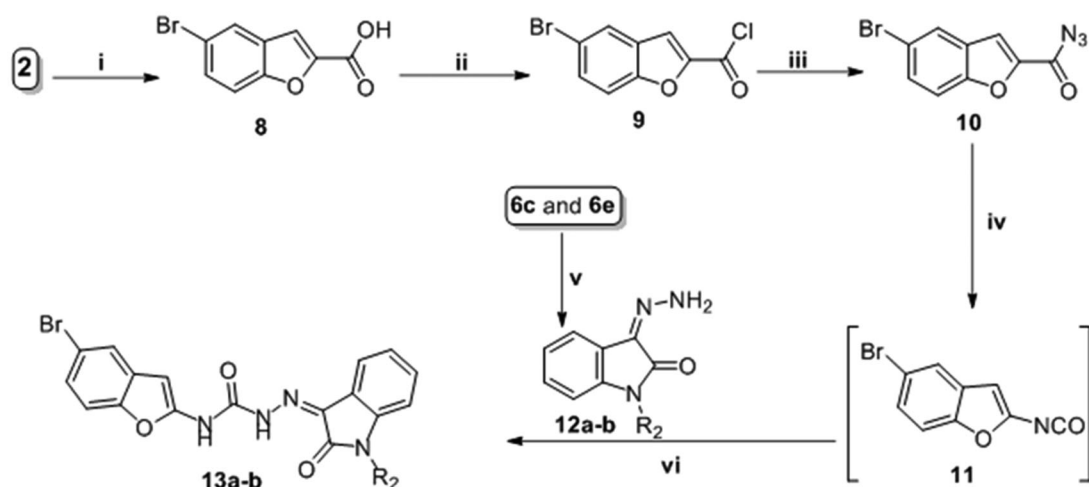
Scheme 3. Synthesis of target compounds **13a-b**; Reagents and conditions: (**i**) HCl/reflux 6 h, (**ii**) (COCl)$_2$/anhydrous toluene/reflux 5 h, (**iii**) NaN$_3$/acetone/stirring r.t. 1 h, (**iv**) Dry toluene/reflux 1 h. (**v**) NH$_2$NH$_2$.H$_2$O/methanol/reflux 3 h, (**vi**) Anhydrous toluene/reflux 4 h.

which then condensed with the key intermediate **3** to afford target compounds **7a-h**.

In the last scheme, the ester moiety of 5-bromobenzofuran-2-carboxylate **2** succumbed to acidic hydrolysis to afford the acid analogue **8**, which was chlorinated with oxalyl chloride in toluene to get the acid chloride derivative **9** that reacted with NaN$_3$ in acetone to produce 5-bromobenzofuran-2-carbonyl azide **10**. The azide derivative **10** was subjugated to Curtius Rearrangement through heating in anhydrous toluene to furnish isocyanate analogue **11**. On the other hand, isatin derivatives **6c** and **6e** were condensed with hydrazine hydrate to release their hydrazone analogue **12a** and **12b**, respectively, which reacted with isocyanate analogue **11** to get the final target compounds **13a-b**.

The structures of all the synthesised compounds were confirmed under the basis of spectral and elemental analyses which were in full agreement with the proposed structures.

2.2. Biological evaluation

All the newly synthesised compounds were initially tested for their anti-proliferative activity against breast cancer cell lines T-47D and MCF-7 in MTT assay. Compounds showed promising anti-proliferative activity were tested for their PK inhibitory activity on the target kinases CDK-2 and GSK-3β. Furthermore, compounds showed prominent activity at cellular level and on enzymes were further evaluated for their effect on cell cycle progression and cell apoptosis in the breast cancer cell line MCF-7.

2.2.1. In vitro anti-proliferative activity

All the newly synthesised benzofuran-oxindole hybrids were screened for their *in vitro* anti-proliferative activity against the breast cancer cell lines T-47D and MCF-7 using the MTT assay, and the results were compared with the pan-kinase inhibitor staurosporine as a reference standard [102]. The IC$_{50}$ values are presented in Table 1.

On MCF-7 cell line, the tested hybrids showed an IC$_{50}$ range of 2.27–37.04 μM, with compounds **5d-f**, **7 b** and **7 h** showing potent cytotoxic effect (3.41, 3.45, 2.27, 2.64 and 4.32 μM, respectively) compared to the reference staurosporine which showed an IC$_{50}$ of 4.81 μM. Compounds **5a**, **7d**, **7e** and **13 b** showed moderate cytotoxic activity with IC$_{50}$ of 5.47, 7.48, 8.33 and 5.70, respectively,

whereas, the rest of compounds showed weak cytotoxic activity with IC$_{50}$ higher than 10 μM (Table 1).

On T-47D cell line, the tested compounds showed an IC$_{50}$ range of 1.27–43.27 μM, with compounds **5 b**, **5d-e**,**7h** and **13a** showing potent cytotoxic effect (IC$_{50}$ of 1.27, 3.82, 4.53, 1.72 and 3.22 μM, respectively) compared to the reference staurosporine which showed an IC$_{50}$ of 4.34 μM. Compounds **5a**, **5c**, **5f**, **5 g** and **7 g** showed moderate cytotoxic activity with IC$_{50}$ of 9.67, 6.03, 7.80, 6.65 and 9.67 μM, respectively, whereas, the rest of compounds showed weak cytotoxic activity with IC$_{50}$ higher than 10 μM (Table 1).

These results indicate the superior cytotoxic activity of the *N*-unsubstituted isatin derivatives **5a-g** on both breast cancer cell lines with IC$_{50}$ range of 2.27–12.93 μM and 1.27–9.67 μM on MCF-7 and T-47D cell lines, respectively, which could be due to their better binding to the target kinases. Compounds **5d–f** with Br, CH$_3$ and OCH$_3$ substituent on the isatin nucleus, respectively, showed the best cytotoxic activity (Table 1).
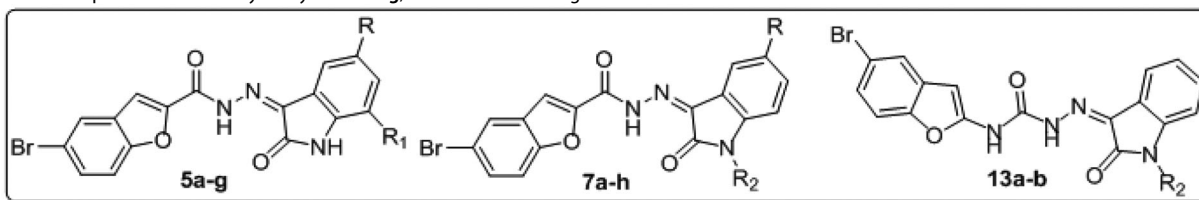
Series **7** showed moderate to weak cytotoxic activity on either or both cell lines, except for the *N*-benzylisatin hybrid **7 h** which showed a potent cytotoxic activity on both cell lines with IC$_{50}$ of 4.32 and 1.72 μM on MCF-7 and T-47D, respectively. These results indicate that the *N*-substitution at the isatin nucleus greatly affects the cytotoxic activity in the newly synthesised compounds mostly in a negative manner (Table 1).

Worthy of note, replacing the amido group in compound **7c** and **7e** with the ureido moiety to afford **13a** and **13 b** greatly enhanced the cytotoxic activity in both cell lines (37.04 and 8.33 μM *vs* 18.21 and 5.70 μM, respectively, in MCF-7) and (43.27 and 11.80 μM *vs* 3.22 and 10.88 μM, respectively, in T-47D) (Table 1).

2.2.2. CDK2 and GSK-3β inhibitory activities

The most potent hybrids on breast cancer cell lines (**series 5**) were further evaluated biochemically for their kinase inhibitory activity on CDK-2 and GSK-3β using their Kinase Assay Kits, and were compared to the pan-kinase inhibitor staurosporine as a reference standard. The results were presented in Table 2.

On CDK2, the tested compounds showed potent sub-micromolar inhibitory activity with IC$_{50}$ ranged from 37.80 to 177 nM in comparison to that of the used reference standard (IC$_{50}$ = 38.50 nM). The bromo isatin derivative **5d** showed the most

Table 1. *In vitro* anti-proliferative activity of hybrids **5a–g**, **7a–h** and **13a–b** against breast T-47D and MCF-7 cancer cell lines.

Comp.	R	R_1	R_2	MCF-7	T-47D
				IC$_{50}$ (µM)^a	
5a	H	H	–	5.47 ± 0.16	9.67 ± 0.31
5b	F	H	–	12.93 ± 0.38	1.27 ± 0.04
5c	Cl	H	–	12.46 ± 0.37	6.03 ± 0.19
5d	Br	H	–	3.41 ± 0.10	3.82 ± 0.12
5e	CH$_3$	H	–	3.45 ± 0.10	4.53 ± 0.14
5f	OCH$_3$	H	–	2.27 ± 0.06	7.80 ± 0.25
5g	CH$_3$	CH$_3$	–	11.95 ± 0.35	6.65 ± 0.21
7a	H	–	CH$_3$	10.43 ± 1.01	11.79 ± 1.05
7b	H	–	CH$_2$CH=CH$_2$	2.64 ± 0.07	12.24 ± 0.40
7c	H	–	CH$_2$CH(CH$_3$)$_2$	37.04 ± 1.87	43.27 ± 2.39
7d	H	–	CH$_2$COOC$_2$H$_5$	7.48 ± 0.22	18.99 ± 0.62
7e	H	–	CH$_2$Ph	8.33 ± 0.24	11.80 ± 0.38
7f	H	–	CH$_2$CH$_2$Ph	24.67 ± 0.72	38.7 ± 1.26
7g	Br	–	CH$_2$CH(CH$_3$)$_2$	24.82 ± 0.73	9.67 ± 0.31
7h	Br	–	CH$_2$Ph	4.32 ± 0.12	1.72 ± 0.04
13a	–	–	CH$_2$CH(CH$_3$)$_2$	18.21 ± 0.53	3.22 ± 0.19
13b	–	–	CH$_2$Ph	5.70 ± 0.16	10.88 ± 0.35
Staurosporine	–	–	–	4.81 ± 0.14	4.34 ± 0.14

^{a}IC$_{50}$ values are the mean ± SD of three separate experiments.

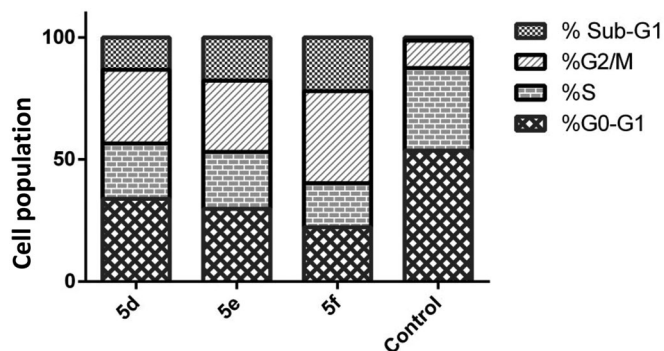**Table 2.** Inhibitory activities of compounds **5a–g** against CDK2 and GSK-3β.

Comp.	CDK2	GSK-3β
	IC$_{50}$ (nM)^a	
5a	140.6 ± 7.7	136.9 ± 7.5
5b	52.46 ± 2.9	212.3 ± 12
5c	85.36 ± 4.6	102 ± 5.6
5d	37.77 ± 2.1	32.09 ± 1.7
5e	176.5 ± 9.6	80.75 ± 4.4
5f	52.75 ± 2.9	40.13 ± 2.2
5g	104.8 ± 5.7	75.54 ± 4.1
Staurosporine	38.5 ± 2.1	43.38 ± 2.4

^{a}IC$_{50}$ values are the mean ± SD of three separate experiments.

Figure 5. Effect of hybrids **5d**, **5e** and **5f** on the phases of cell cycle of MCF-7 cells.

potent inhibitory activity with IC$_{50}$ of 37.80 nM comparable to that of staurosporine. Compounds **5b**, **5c** and **5f** showed two-digit nanomolar inhibitory activity with IC$_{50}$ of 52.50, 85.40 and 52.80, respectively (Table 2).

On GSK-3β, the tested compounds showed potent sub-micromolar inhibitory activity as well with IC$_{50}$ range of 32.09–212.30 nM in comparison to the used reference standard (IC$_{50}$ = 43.38 nM). The bromo isatin **5d** and the methoxy isatin **5f** derivative showed more potent inhibitory activity than that of staurosporine (IC$_{50}$ of 32.09 and 40.13 nM, respectively). Compounds **5e** and **5g** showed two-digit nanomolar inhibitory activity with IC$_{50}$ of 75.54 and 80.75 nM, respectively (Table 2).

These results indicate the superiority of the bromo isatin **5d** and the methoxy isatin **5f** derivatives on both kinases (Table 2). The methyl isatin derivative **5e** shows a relatively less kinase inhibitory activity than its bromo **5d** and methoxy **5f** congeners on both kinases despite of its obvious potent cellular cytotoxicity which could be attributed to its probable further cytotoxic mechanisms besides CDK2/GSK-3β dual inhibition.

2.2.3. Cell cycle analysis

Cyclin E/CDK2 complexation plays an important role at G1 phase, whereas, cyclin A/CDK2 complexation terminates S phase and drives the cell cycle through normal G2/M phase progression[25,37,103,104]. Furthermore, a significant percentage of CDK2-deficient cells arrest in the G2/M phase, additionally, breast cancer cells exposed to CDK2 inhibitors show G2/M phase arrest[23,105]. In the same vein, GSK-3β regulates the strength of the mitotic checkpoint and connects the PI3K and WNT-signalling pathways to mitosis, furthermore, GSK-3β inhibitors induce G2/M phase arrest as well[30,106,107].

Compounds showing promising antiproliferative as well as kinase inhibitory activity **5d**, **5e** and **5f** were further investigated for their influence on the cell cycle progression by flow cytometry analysis using propidium iodide (PI) stain. Cell cycle parameters were compared for the breast cancer MCF-7 cells with DMSO as control and after treatment with the compounds of interest and

incubation for 24 h, and the results were presented in Figure 5 and Table 3.

From the obtained results Figure 5 and Table 3, it is noticeable that there is an increase in the percent of cell distribution in the G2/M phase, from 11.30% in control to 30.26, 29.21 and 37.82% in treated cells with **5d**, **5e** and, **5f**, respectively, indicating a G2/M phase arrest which is the expected consequence from CDK2/GSK-3β dual inhibition confirming the mechanism of action of the designed compounds on the target kinases. Furthermore, an increase in the percent of cells accumulated in the sub-G1 phase, from 1.29% in the control to 13.27, 17.73 and 22.02% in the treated cells with **5d**, **5e** and, **5f**, respectively, as a result of cell apoptosis.

The high efficacy of compound **5f** in cell arrest at G2/M phase and in cell apoptosis as indicated by its results in Table 3 relative to its congeners **5d** and **5e** aligns with its potent effect on MCF-7 as indicated by its IC$_{50}$ (2.27 μM) in comparison to the IC$_{50}$ of compounds **5d** and **5e** (3.41 and 3.45 μM, respectively).

2.2.4. Apoptosis assay

To investigate further the effect of the promising compounds **5d**, **5e**, and **5f** on cell apoptosis, Annexin V-FITC/propidium iodide dual staining assay was performed according to the reported method[108]. The morphological markers of apoptosis in the breast cancer MCF-7 cell line were examined before and after treatment with the compounds of interest. Apoptosis assay depends on the translocation of the phosphatidylserine (PS) phospholipid to the cell surface in cells undergoing apoptosis which can be easily detected by staining with the fluorescent conjugate of annexin V followed by flow cytometry analysis. Simultaneously, MCF-7 cells were stained with propidium iodide (PI) which could enter cells with damaged plasma membranes only. This enables the discrimination between early apoptotic cells (positive for PS, but negative for PI) from late apoptotic and necrotic cells (positive for both PS and PI).

Figure 6 and Table 4 show that the percentage of the total apoptotic cells in MCF-7 cell line increases after treatment with

compounds **5d**, **5e**, and **5f** (13.75, 19.74, and 26.10%, respectively) relative to control cells (0.82%) which is a significant indication of the apoptotic effect of the compounds of interest. Compounds **5d**, **5e**, and **5f** produced an increase in the early apoptotic phase, from 0.63 to 3.61, 4.66, and 3.94, respectively, and an increase in the late apoptotic phase, from 0.19 to 10.14, 15.08, and 22.16, respectively.

2.2.5. Cytotoxicity towards non-tumorigenic cells

In order to investigate their selectivity on cancer cells, hybrids **5d**, **5e** and **5f**, endowed with dual growth inhibitory action against MCF-7 and T-47D cells, were assesses for their cytotoxic action towards the non-tumorigenic breast cells (MCF-10A), via the MTT assay. The obtained IC$_{50}$s and the calculated mean tumour selectivity index (S.I.); IC$_{50}$ for MCF-10A/IC$_{50}$ average for (MCF-7 and T-47D) have been presented in Table 5. The examined hybrids exerted weak cytotoxic effect (IC$_{50}$ = 21.66 ± 1.05, 23.59 ± 0.86 and 39.95 ± 1.42 μM, respectively, with selectivity indexes equal 6.0, 5.9 and 7.9, respectively, Table 5.

## 3. Molecular docking study and structure activity relationship

In the present molecular docking study, a pair of protein structures were used for CDK2 and GSK-3β, viz, PDB ID: 1FVT[109] and

Table 3. Effect of compounds **5d**, **5e** and **5f** on the phases of cell cycle of MCF-7 cells

Comp.	%G0-G1	%S	%G2/M	%Sub-G1
5d	33.97	22.5	30.26	13.27
5e	29.85	23.21	29.21	17.73
5f	22.28	17.88	37.82	22.02
Control	53.59	33.82	11.3	1.29

Table 4. Distribution of apoptotic cells in the AnnexinV-FITC/PI dual staining assay in MCF-7 cells upon treatment with compounds **5d**, **5e** and **5f**.

Comp.	Total (L.R % + U.R %)	Early Apoptosis (Lower Right %)	Late Apoptosis (Upper Right %)	Necrosis
5d	13.75	3.61	10.14	1.56
5e	19.74	4.66	15.08	1.81
5f	26.10	3.94	22.16	2.14
Control	0.82	0.63	0.19	0.49

Table 5. Cytotoxic action for hybrids **5d**, **5e** and **5f** towards non-tumorigenic breast cell line (MCF-10A), and mean tumour selectivity index (S.I.) (MCF-10A/MCF-7 and T-47D).

	IC$_{50}$ (μM)			
Comp.	MCF-10A	MCF-7	T-47D	Mean tumour selectivity
5d	21.66 ± 1.05	3.41 ± 0.10	3.82 ± 0.12	6.0
5e	23.59 ± 0.86	3.45 ± 0.10	4.53 ± 0.14	5.9
5f	39.95 ± 1.42	2.27 ± 0.06	7.80 ± 0.25	7.9
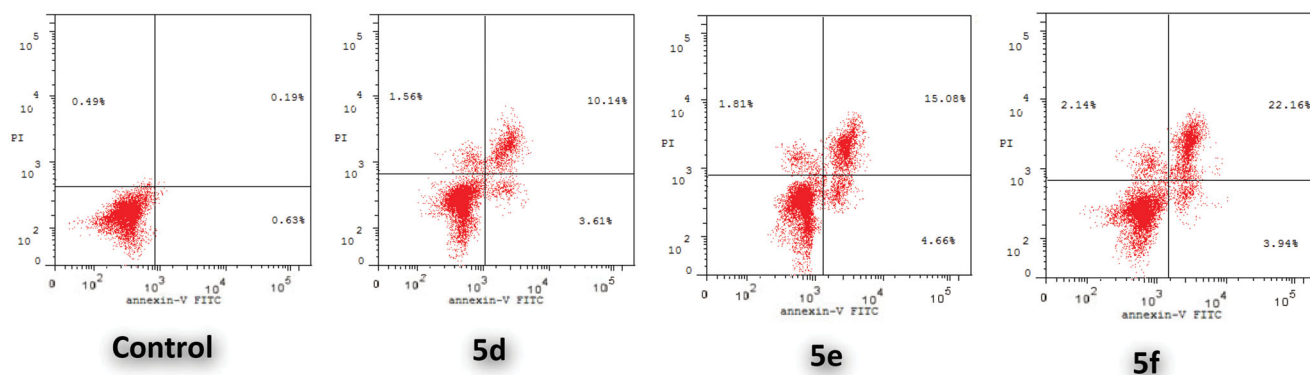
Figure 6. Effect of **5d**, **5e** and **5f** on the percentage of annexin V-FITC-positive staining in MCF-7 cells. The experiments were done in triplicates. The four quadrants identified as: **LL**, viable; **LR**, early apoptotic; **UR**, late apoptotic; **UL**, necrotic.

(A)

(B)
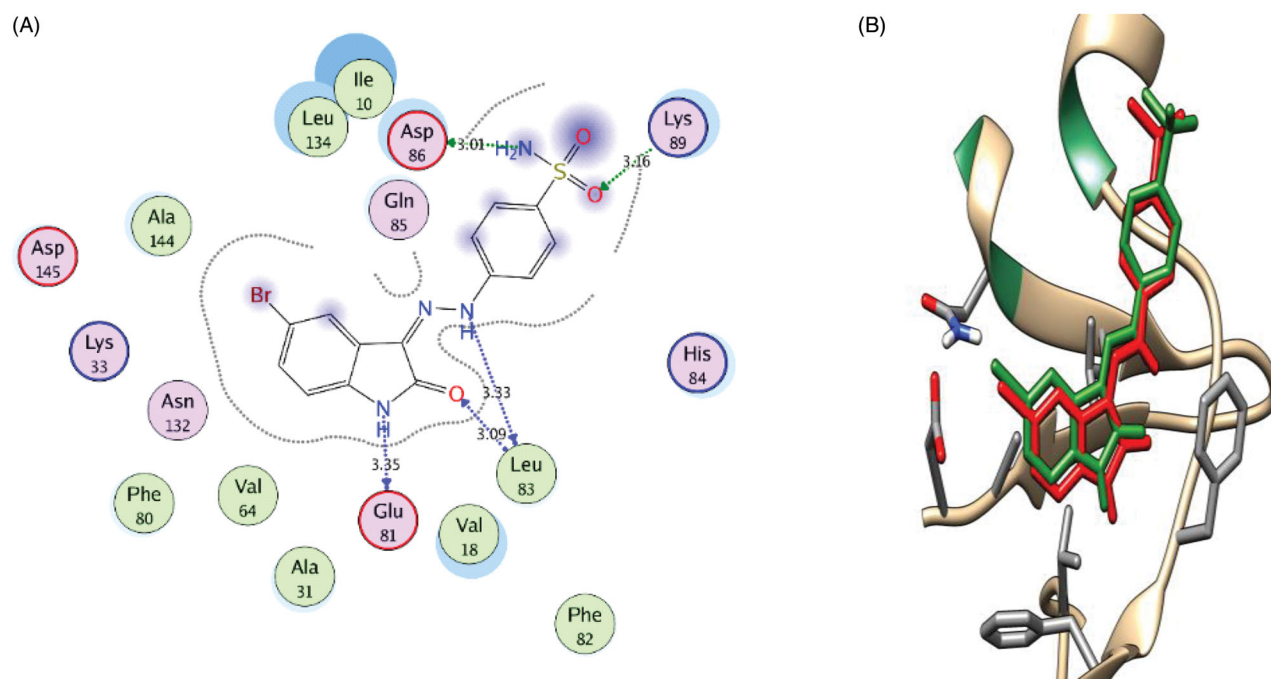
Figure 7. (**A**) 2 D interaction diagram showing the oxindole derivative docking pose interactions with the key amino acids (hot spots) in the CDK2 active site. (Distances in Å) (**B**) 3 D representations of the superimposition of the docking pose (green) and the co-crystallized pose (red) of the oxindole derivative in the CDK2 active site, respectively, with RMSD of 0.894 Å.

(A)

(B)
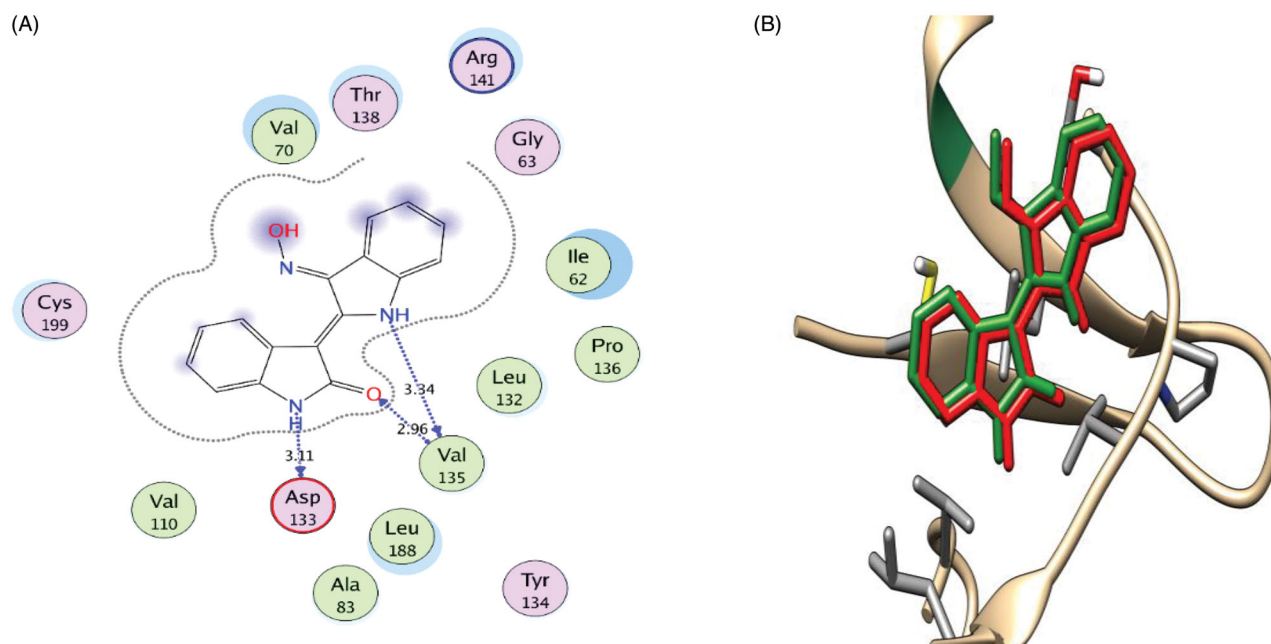
Figure 8. (**A**) 2 D interaction diagram showing Indirubin-3'-monoxime docking pose interactions with the key amino acids (hot spots) in the GSK-3β active site. (Distances in Å) (**B**) 3 D representations of the superimposition of the docking pose (green) and the co-crystallized pose (red) of Indirubin-3'-monoxime in the GSK-3β active site, respectively, with RMSD of 0.471 Å.

PDB ID: 1Q41[110], respectively, which are co-crystallized with potent CDK2 and GSK-3β oxindole-based inhibitors, respectively. Molecular docking was carried out to investigate the interaction of the designed hybrid compounds with CDK2 and GSK-3β kinase domain to rationalise their biological activity, to reveal their probable binding pattern and to elicit their SAR.

Initially, self-docking of the co-crystallized ligands in CDK2 and GSK-3β active sites was performed to validate the used molecular docking protocol. The self-docking step stimulated the binding pattern of the

co-crystallized ligands accurately indicating the suitability of the used docking setup for the planned simulations. This was demonstrated by the small RMSD between the docked and the co-crystallized ligand poses in CDK2 (0.894 Å) and GSK-3β (0.471 Å), and by the ability of the attained docking poses to simulate the main interactions achieved by the co-crystallized ligands with the key amino acids in CDK2 and GSK-3β active sites (Figures 7 and 8, respectively).

In the CDK2 active site the docking pose of the oxindole derivative reproduced the key interactions of the co-crystallized

(A)

(B)
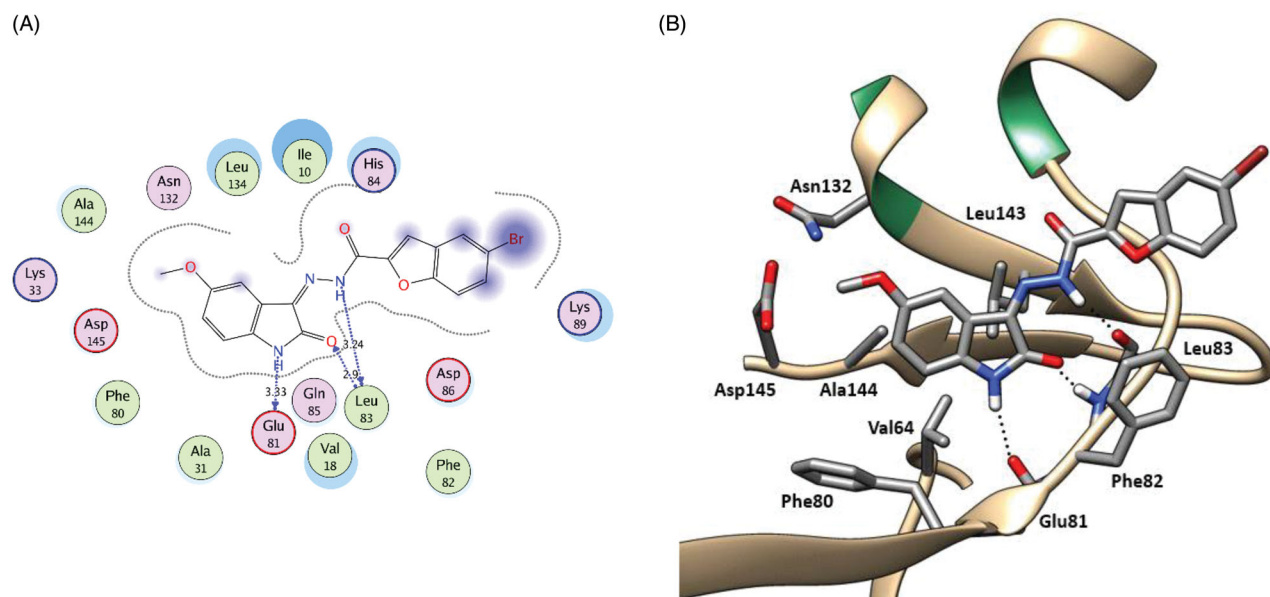
Figure 9. 2 D diagram (A) and 3 D representation (B) of compound **5f** showing its interaction with the CDK2 active site.

(A)

(B)
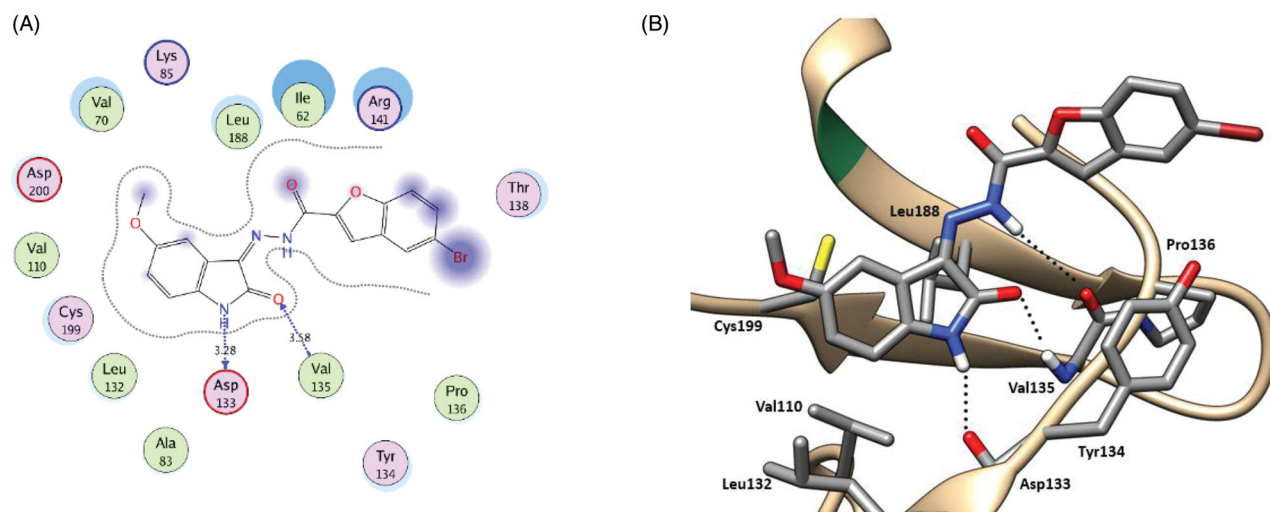
Figure 10. 2 D diagram (A) and 3 D representation (B) of compound **5f** showing its interaction with the GSK-3β active site.

Table 6. Docking energy scores (S) in kcal/mol for the newly synthesised hybrid compounds and the co-crystalized compounds in CDK2 and GSK-3β kinase domain

Compound	Energy score (S) kcal/mol CDK2	Energy score (S) kcal/mol GSK-3β
5a	−9.53	−9.99
5b	−9.89	−10.40
5c	−10.07	−10.59
5d	−10.22	−10.81
5e	−10.05	−10.53
5f	−10.35	−10.96
5g	−10.39	−10.60
7a	−9.19	−10.40
7b	−9.61	−10.24
7c	−10.03	−11.48
7d	−10.21	−11.76
7e	−9.98	−11.58
7f	−10.05	−10.68
7g	−10.56	−11.27
7h	−10.40	−11.46
13a	−13.60	−11.77
13b	−14.72	−11.92
Co-crystalized ligand	−10.63	−12.00

ligand with the active site; it interacts in the hinge region through hydrogen bonding with Glu81 backbone CO and Leu83 backbone NH and CO. Furthermore, its sulfonamidophenylhydrazone group projected outward towards the bulk solvent with the sulphonamide group interacting with Asp86 backbone NH and side-chain carboxyl group and Lys89 side chain NH_3^+ (Figure 7).

As for GSK-3β, the docking pose of indirubin-3′-monoxime reproduced the key interactions of the co-crystalized ligand with the active site; it interacts in the hinge region through hydrogen bonding with Asp133 backbone CO and Val135 backbone NH and CO (Figure 8). Furthermore, through a water mediated hydrogen bonding network, it interacts with Gln185 and Thr138 by its oxime group which is responsible for its selectivity towards GSK-3β over CDK2.

In series **5**, the newly synthesised N^1-unsubstituted oxindole hybrids showed comparable binding patterns in both kinases (Figures 9 and 10 and for further details, see supporting materials). The oxindole ring is accommodated in the hinge region interacting through hydrogen bonding by its NH and CO with the backbone CO and NH of the key amino acids Glu81 and Leu83,

respectively, in CDK2, and Asp133 and Val135, respectively, in GSK-3β.

Moreover, through hydrophobic interaction the fused phenyl ring of the oxindole nucleus interacts with the hydrophobic side chains of the surrounding amino acids; Val18, Ala31, Val64, Phe80, Leu134, and Ala144 in CDK2 and Val70, Ala83, Val110, Leu132, Leu188, and Cys199 in GSK-3β (Figures 9 and 10 and for further details, see supporting materials). Therefore, increasing the substituent hydrophobicity on the oxindole nucleus enhances the binding affinity which is well reflected in the docking binding score and further in the biological activity (Br, **5d** > Cl, **5c** ≈ CH$_3$, **5e** > F, **5b**) (Tables 1, 2 and 6). The remarkable binding affinity of the relatively polar methoxy group (OCH$_3$, **5f**) is attributed to the fact that it is directed towards the bulk solvent and so decreased the solvation penalty during the binding scenario resulting in a considerable increase in the binding affinity. On the other hand, despite of its relatively higher hydrophobicity, the dimethyl substituted hybrid **5g** does not show significant predicted binding score or experimental biological activity what could be attributed to the C^7 methyl substituent which sterically clashes with the bottom of the hinge region hindering the key interaction of the NH and CO of the oxindole ring with the key amino acids; Glu81 and Leu83 in CDK2, respectively, and Asp133 and Val135 in GSK-3β, respectively (For further details, see supporting materials).

The hydrazono linker NH interacts through hydrogen bonding with the backbone CO of Leu83 and Val135 in CDK2 and GSK-3β, respectively, projecting the benzofuran moiety outward towards the bulk solvent which is involved in a hydrophobic interaction with the hydrophobic side chains of the surrounding amino acids lining the gate of the hinge region; Ile10, Phe82, and Leu298 in CDK2 and Ile62, Tyr134 and Pro136 in GSK-3β (Figures 9 and 10 and for further details, see supporting materials).

In series **7** and **13**, the N^1-substitutions on the oxindole nucleus hinder the compounds from achieving the key interactions with hinge region amino acids; Glu81 and Leu83 in CDK2, and Asp133 and Val135 in GSK-3β what rationalises their moderate to low antiproliferative activity (For further details, see supporting materials). Molecular docking simulations show their non-selective bindings and random binding patterns what rationalise their low activity despite of their good docking binding scores (Table 6).

These results point out the criticality of N^1 being unsubstituted for CDK2/GSK-3β kinase inhibition. The N^1-benzyloxindole derivative **7h** showing promising antiproliferative activity might be exerting its effect through other mechanism than CDK2/GSK-3β kinase inhibition.

4. Conclusions

In the present study three series of oxindole-benzofuran hybrids were designed and synthesised as dual CDK2/GSK-3β inhibitors targeting breast cancer (**5a-g**, **7a-h**, and **13a-b**). In MTT assay on the breast cancer cell lines MCF-7 and T-47D, the N^1-unsubstituted oxindole derivatives, **series 5**, showed moderate to potent activity on both breast cancer cell lines. Compounds **5d-f** showed the most potent cytotoxic activity with IC$_{50}$ of 3.41, 3.45 and 2.27 μM, respectively, on MCF-7 and IC$_{50}$ of 3.82, 4.53 and 7.80 μM, respectively, on T-47D cell lines, in comparison to the used reference standard (staurosporine) IC$_{50}$ of 4.81 and 4.34 μM, respectively. On the other hand, the N^1-substituted oxindole derivatives, **series 7 and 13**, showed moderate to weak cytotoxic activity on both breast cancer cell lines except for compound **7h** which showed potent antiproliferative activity with IC$_{50}$ of 4.32 and 1.72 μM on

MCF-7 and T-47D cell lines, respectively. CDK2 and GSK-3β inhibition testing of the potent **series 5** indicated that compounds **5d** and **5f** exhibit potent dual CDK2/GSK-3β inhibitory activity with IC$_{50}$ of 37.77 and 52.75 nM, respectively, on CDK2 and 32.09 and 40.13 nM, respectively, on GSK-3β. The most potent hybrids **5d-f** triggered cell cycle arrest in the G2/M phase as a consequence of their dual CDK2/GSK-3β inhibition. Moreover, compounds **5d-f** induced apoptosis in MCF-7 cells as indicated by the percent of the total apoptosis of 13.75, 19.74, and 26.10%, respectively, in comparison to the untreated cells which showed 0.82% total apoptosis. The molecular docking study showed that the newly synthesised N^1-unsubstituted oxindole hybrids have comparable binding patterns in both CDK2 and GSK-3β. The oxindole ring is accommodated in the hinge region interacting through hydrogen bonding with the backbone CO and NH of the key amino acids Glu81 and Leu83, respectively, in CDK2 and Asp133 and Val135, respectively, in GSK-3β. Moreover, through hydrophobic interaction the fused phenyl ring of the oxindole nucleus interacts with the hydrophobic side chains of the surrounding amino acids; Val18, Ala31, Val64, Phe80, Leu134, and Ala144 in CDK2 and Val70, Ala83, Val110, Leu132, Leu188, and Cys199 in GSK-3β. The hydrazono linker NH interacts through hydrogen bonding with the backbone CO of Leu83 and Val135 in CDK2 and GSK-3β, respectively, projecting the benzofuran moiety outward towards the bulk solvent which is involved in a hydrophobic interaction with the hydrophobic side chains of the surrounding amino acids lining the gate of the hinge region; Ile10, Phe82, and Leu298 in CDK2 and Ile62, Tyr134 and Pro136 in GSK-3β. In series **7** and **13**, the N^1-substitutions on the oxindole nucleus hinder the compounds from achieving the key interactions with hinge region amino acids; Glu81 and Leu83 in CDK2, and Asp133 and Val135 in GSK-3β what rationalises their moderate to low antiproliferative activity.

5. Experimental

5.1. Chemistry

5.1.1. General
Melting points were measured with a Stuart melting point apparatus and were uncorrected. Infra-red spectra were recorded on Schimadzu FT-IR 8400S spectrophotometer. The NMR spectra were recorded by Bruker spectrometer at 400 MHz. ^{13}C NMR spectra were run at 100 MHz in deuterated dimethylsulphoxide (DMSO$d6$). Elemental analyses were carried out at the Regional Centre for Microbiology and Biotechnology, Al-Azhar University, Cairo, Egypt. Unless otherwise noted, all solvents and reagents were commercially available and used without further purification. Compounds (**2** and **3**)[97], (**6a–h**)[111–112], (**8–9**)[113], and (**12 b**)[114] were prepared according to the reported methods.

5.1.1.2. Synthesis of 5-bromobenzofuran-2-carbohydrazide 3.
To hot stirred solution of ethyl 5-bromobenzofuran-2-carboxylate **2** (1 g, 3.7 mmol) in 30 ml of methanol, hydrazine hydrate (0.25 ml, 7.5 mmol) was added. The reaction solution was left for heating under reflux for 4 h, and then poured onto cold water. The formed solid was collected by filtration, washed with diethyl ether and recrystallized from EtOH/DMF mixture to furnish the key intermediate **3**.

5.1.1.3. Synthesis of target compounds 5a–g and 7a–h.
5-Bromobenzofuran-2-carbohydrazide **3** (0.3 g, 1.2 mmol) was added to a hot solution of equivalent amount of the appropriate isatin

derivative (**4a–g** or **6a–h**) in ethanol (15 ml) with catalytic amount of ethanoic acid. The reaction mixture was heated under reflux for 4–7 h with TLC monitoring, once the reaction completed, the reaction mixture was left for cooling then was filtered-off. The produced solid was washed with water, diethyl ether and recrystallized from dioxane/propanol mixture to produce target compounds **5a–g** and **7a–h**, respectively.

5.1.1.3.1. 5-Bromo-N′-(2-oxoindolin-3-ylidene)benzofuran-2-carbohydrazide 5a. Yellow powder (yield 75%), m.p. > 300 °C; ^{1}H NMR *ppm*: 6.94–7.00 (m, 1H, Ar-H), 7.11 (t, 1H, Ar-H, $J=8.0$ Hz), 7.41–7.47 (m, 1H, Ar-H), 7.64–7.84 (m, 3H, Ar-H), 7.99 (t, 1H, Ar-H, $J=8.0$ Hz), 8.09, 8.11 (2 s, 1H, Ar-H), 10.91, 11.39 (2 s, 1H, NH indolin-2-one), 11.89, 14.06 (2 s, 1H, NH); ^{13}C NMR δ *ppm*: 111.32, 114.73, 116.72, 120.10, 121.76, 122.45, 123.30, 126.13, 127.23, 129.61, 131.18, 132.70, 133.70, 143.29, 153.87, 163.35 (C=O indolin-2-one), 165.04 (C=O hydrazide); IR (KBr, ν cm^{-1}) 3380, 3345 (2NH) and 1711, 1701 (2 C=O); MS *m/z* [%]: 384 [M$^+$+2, 50.94], 382 [M$^+$, 48.60], 160 [100]; Analysis calculated for $C_{17}H_{10}BrN_3O_3$: C, 53.15; H, 2.62; N, 10.94; found C, 53.33; H, 2.64; N, 10.82.

5.1.1.3.2. 5-Bromo-N′-(5-fluoro-2-oxoindolin-3-ylidene)benzofuran-2-carbohydrazide 5b. Red powder (yield 77%), m.p. > 300 °C; ^{1}H NMR *ppm*: 6.92–7.00 (m, 1H, Ar-H), 7.24–7.33 (m, 1H, Ar-H), 7.49, 7.86 (2br s, 1H, Ar-H), 7.67–7.71 (m, 1H, Ar-H), 7.74 (t, 1H, Ar-H, $J=8.0$ Hz), 7.96 (d, 0.6H, Ar-H, $J=8.0$ Hz), 8.04–8.13 (m, 1.4H, Ar-H), 10.92, 11.42 (2 s, 1H, NH indolin-2-one), 12.02, 14.02 (2 s, 1H, NH); IR (KBr, ν cm^{-1}) 3280, 3245 (2NH) and 1723, 1705 (2 C=O); Analysis calculated for $C_{17}H_9BrFN_3O_3$: C, 50.77; H, 2.26; N, 10.45; found C, 50.90; H, 2.24; N, 10.57.

5.1.1.3.3. 5-Bromo-N′-(5-chloro-2-oxoindolin-3-ylidene)benzofuran-2-carbohydrazide 5c. Orange powder (yield 83%), m.p. > 300 °C; ^{1}H NMR *ppm*: 6.94–7.01 (m, 1H, Ar-H), 7.45–7.50 (m, 1H, Ar-H), 7.64–7.76 (m, 2.3H, Ar-H), 8.04, 8.10 (2 s, 1H, Ar-H), 8.14–8.17 (m, 1.7H, Ar-H), 11.03, 11.50 (2 s, 1H, NH indolin-2-one), 12.08, 13.96 (2 s, 1H, NH); ^{13}C NMR δ *ppm*: 112.66, 114.60, 116.94, 118.92, 121.28, 124.34, 126.29, 126.77, 131.04, 132.93, 137.31, 141.43, 143.41, 153.82, 163.17 (C=O indolin-2-one), 164.88 (C=O hydrazide); IR (KBr, ν cm^{-1}) 3300, 3240 (2NH) and 1735, 1702 (2 C=O); Analysis calculated for $C_{17}H_9BrClN_3O_3$: C, 48.77; H, 2.17; N, 10.04; found C, 48.82; H, 2.16; N, 9.93.

5.1.1.3.4. 5-Bromo-N′-(5-bromo-2-oxoindolin-3-ylidene)benzofuran-2-carbohydrazide 5d. Orange powder (yield 87%), m.p. > 300 °C; ^{1}H NMR *ppm*: 6.91–6.97 (m, 1H, Ar-H), 7.60 (d, 1H, Ar-H, $J=8.0$ Hz), 7.71–7.76 (m, 2H, Ar-H), 8.03–8.15 (m, 2H, Ar-H), 8.31 (s, 1H, Ar-H), 11.05, 11.52 (2 s, 1H, NH indolin-2-one), 12.09, 13.99 (2 s, 1H, NH); IR (KBr, ν cm^{-1}) 3295, 3271 (2NH) and 1732, 1701 (2 C=O); Analysis calculated for $C_{17}H_9Br_2N_3O_3$: C, 44.09; H, 1.96; N, 9.07; found C, 43.81; H, 1.98; N, 9.16.

5.1.1.3.5. 5-Bromo-N′-(5-methyl-2-oxoindolin-3-ylidene)benzofuran-2-carbohydrazide 5e. Brown powder (yield 84%), m.p. > 300 °C; ^{1}H NMR *ppm*: 2.23, 2.35 (2 s, 3H, CH$_3$), 6.84–6.88 (m, 1H, Ar-H), 7.22–7.27 (m, 1H, Ar-H), 7.47 (s, 0.6H, Ar-H), 7.68–7.71 (m, 1H, Ar-H), 7.74–7.79 (m, 1H, Ar-H), 7.82–7.88 (m, 1H, Ar-H), 8.00 (s, 0.4H, Ar-H), 8.09–8.14 (m, 1H, Ar-H), 10.80, 11.28 (2 s, 1H, NH indolin-2-one), 11.83, 14.05 (2 s, 1H, NH) ; ^{13}C NMR δ *ppm*: 20.97 (CH$_3$), 111.57, 114.65, 116.89, 120.09, 122.08, 126.14, 127.54, 129.60, 130.92, 131.15, 132.44, 133.12, 141.02, 142.44, 153.84, 163.41 (C=O indolin-2-one), 165.09 (C=O hydrazide); IR (KBr, ν cm^{-1}) 3320, 3341 (2NH) and 1721, 1700 (2 C=O); Analysis calculated for $C_{18}H_{12}BrN_3O_3$: C, 54.29; H, 3.04; N, 10.55; found C, 54.57; H, 3.01; N, 10.62.

5.1.1.3.6. 5-Bromo-N′-(5-methoxy-2-oxoindolin-3-ylidene)benzofuran-2-carbohydrazide 5f. Red powder (yield 82%), m.p. > 300 °C; ^{1}H NMR *ppm*: 3.80, 3.83 (2 s, 3H, OCH$_3$), 6.85–6.91 (m, 1H, Ar-H), 6.98–7.07 (m, 1H, Ar-H), 7.18 (s, 1H, Ar-H), 7.68–7.76 (m, 2H, Ar-H), 7.82, 8.01 (2 s, 1H, Ar-H), 8.08–8.13 (m, 1H, Ar-H), 10.72, 11.20 (2 s, 1H, NH indolin-2-one), 11.97, 14.10 (2 s, 1H, NH); IR (KBr, ν cm^{-1}) 3324, 3301 (2NH) and 1718, 1710 (2 C=O); MS *m/z* [%]: 416 [M$^+$+2, 75.42], 414 [M$^+$, 77.51], 402 [100]; Analysis calculated for $C_{18}H_{12}BrN_3O_4$: C, 52.19; H, 2.92; N, 10.14; found C, 52.01; H, 2.95; N, 10.25.

5.1.1.3.7. 5-Bromo-N′-(5,7-dimethyl-2-oxoindolin-3-ylidene)benzofuran-2-carbohydrazide 5g. Red powder (yield 76%), m.p. > 300 °C; ^{1}H NMR *ppm*: 2.20, 20.22 (2 s, 3H, CH$_3$ of C-7 of indolin-2-one), 2.29, 2.32 (2 s, 3H, CH$_3$ of C-5 of indolin-2-one), 7.06, 7.11 (2 s, 1H, Ar-H), 7.30 (s, 0.5H, Ar-H), 7.69–7.71 (m, 1.5H, Ar-H), 7.75–7.79 (m, 1H, Ar-H), 7.82, 8.00 (2 s, 1H, Ar-H), 8.09, 8.11 (2 s, 1H, Ar-H), 10.82, 11.29 (2 s, 1H, NH indolin-2-one), 11.78, 14.06 (2 s, 1H, NH); ^{13}C NMR δ *ppm*: 16.31 (CH$_3$ C-7 of indolin-2-one), 20.88 (CH$_3$ C-5 of indolin-2-one), 114.67, 116.88, 119.47, 120.97, 123.31, 126.13, 129.61, 131.11, 132.34, 134.53, 135.97, 139.65, 141.47, 142.47, 153.84, 163.82 (C=O indolin-2-one), 165.16 (C=O hydrazide); IR (KBr, ν cm^{-1}) 3350, 3315 (2NH) and 1723, 1701 (2 C=O); MS *m/z* [%]: 414 [M$^+$+2, 17.45], 412 [M$^+$, 14.19], 160 [100]; Analysis calculated for $C_{19}H_{14}BrN_3O_3$: C, 55.36; H, 3.42; N, 10.19; found C, 55.53; H, 3.38; N, 10.27.

5.1.1.3.8. 5-Bromo-N′-(1-methyl-2-oxoindolin-3-ylidene)benzofuran-2-carbohydrazide 7a. Yellow powder (yield 81%), m.p. 260–262 °C; ^{1}H NMR *ppm*: 3.27 (s, 3H, N-CH$_3$), 7.19 (t, 2H, Ar-H, $J=8.0$ Hz), 7.50 (t, 1H, Ar-H, $J=8.0$ Hz), 7.68–7.71 (m, 2H, Ar-H), 7.76 (d, 1H, Ar-H, $J=8.0$ Hz), 7.85 (s, 1H, Ar-H), 8.09 (s, 1H, Ar-H), 11.97, 14.02 (2 s, 1H, NH); ^{13}C NMR δ *ppm*: 26.26 (N-CH$_3$), 110.59, 114.68, 116.94, 119.40, 121.41, 123.84, 126.16, 129.60, 130.33, 131.24, 132.62, 138.18, 144.51, 151.44, 153.87, 161.58 (C=O indolin-2-one), 165.10 (C=O hydrazide); IR (KBr, ν cm^{-1}) 3345 (NH) and 1720, 1695 (2 C=O); MS *m/z* [%]: 400 [M$^+$+2, 92.41], 398 [M$^+$, 94.85], 91 [100]; Analysis calculated for $C_{18}H_{12}BrN_3O_3$: C, 54.29; H, 3.04; N, 10.55; found C, 54.48; H, 3.02; N, 10.64.

5.1.1.3.9. N′-(1-Allyl-2-oxoindolin-3-ylidene)-5-bromobenzofuran-2-carbohydrazide 7b. Orange powder (yield 73%), m.p. 207–209 °C; ^{1}H NMR *ppm*: 4.46 (s, 2H, N-CH$_2$), 5.22–5.31 (m, 2H, =CH$_2$), 5.88–5.97 (m, 1H, N-CH$_2$-CH), 7.13 (d, 1H, Ar-H, $J=8.0$ Hz), 7.19 (t, 1H, Ar-H, $J=8.0$ Hz), 7.47 (t, 1H, Ar-H, $J=8.0$ Hz), 7.68–7.72 (m, 2H, Ar-H), 7.76 (d, 1H, Ar-H, $J=8.0$ Hz),) , 7.85 (s, 1H, Ar-H), 8.09 (s, 1H, Ar-H), 11.99, 13.97 (2 s, 1H, NH); IR (KBr, ν cm^{-1}) 3304 (NH) and 1715, 1701 (2 C=O); Analysis calculated for $C_{20}H_{14}BrN_3O_3$: C, 56.62; H, 3.33; N, 9.90; found C, 56.77; H, 3.31; N, 10.01.

5.1.1.3.10. 5-Bromo-N′-(1-isobutyl-2-oxoindolin-3-ylidene)benzofuran-2-carbohydrazide 7c. Yellow powder (yield 65%), m.p. 216–218 °C; ^{1}H NMR *ppm*: 0.94 (d, 6H, -CH-(CH$_3$)$_2$, $J=8.0$ Hz), 2.09–2.16 (m, 1H, N-CH$_2$-CH), 3.36 (d, 2H, N-CH$_2$, $J=8.0$ Hz), 7.17 (t, 1H, Ar-H, $J=8.0$ Hz), 7.24 (d, 1H, Ar-H, $J=8.0$ Hz), 7.47 (t, 1H, Ar-H, $J=8.0$ Hz), 7.67–7.70 (m, 2H, Ar-H), 7.77 (d, 1H, Ar-H, $J=8.0$ Hz), 7.84 (s, 1H, Ar-H), 8.08 (s, 1H, Ar-H), 13.99 (s, 1H, NH); IR (KBr, ν cm^{-1}) 3312 (NH) and 1720, 1711 (2 C=O); Analysis calculated for

$C_{21}H_{18}BrN_3O_3$: C, 57.29; H, 4.12; N, 9.54; found C, 57.08; H, 4.17; N, 9.47.

5.1.1.3.11. Ethyl-2–(3-(2–(5-bromobenzofuran-2-carbonyl)hydrazono)-2-oxoindolin-1-yl)acetate 7d.

Orange powder (yield 69%), m.p. 215–216 °C; ^{1}H NMR ppm: 1.23 (t, 3H, CH$_3$, J = 8.0 Hz), 4.18 (q, 2H, CH$_2$, J = 8.0 Hz), 4.76 (s, 2H, N-CH$_2$), 7.22 (t, 1H, Ar-H, J = 8.0 Hz), 7.50 (t, 1H, Ar-H, J = 8.0 Hz), 7.96–7.78 (m, 2H, Ar-H), 7.87 (s, 1H, Ar-H), 8.10 (s, 1H, Ar-H), 13.81 (s, 1H, NH); ^{13}C NMR δ ppm: 14.49 (CH$_3$), 41.47 (-CH$_2$-CH$_3$), 61.97 (N-CH$_2$), 110.93, 113.40, 114.68, 116.96, 119.28, 121.62, 124.20, 124.67, 126.19, 129.59, 131.33, 132.68, 143.48, 150.87, 153.88, 161.55 (C=O indolin-2-one), 165.22 (C=O hydrazide), 167.89 (C=O ester); IR (KBr, ν cm^{-1}) 3324 (NH) and 1745, 1715, 1698 (3 C=O); Analysis calculated for $C_{21}H_{16}BrN_3O_5$: C, 53.63; H, 3.43; N, 8.94; found C, 53.80; H, 3.42; N, 8.88.

5.1.1.3.12. N′-(1-Benzyl-2-oxoindolin-3-ylidene)-5-bromobenzofuran-2-carbohydrazide 7e.

Yellow powder (yield 80%), m.p. 248–250 °C; ^{1}H NMR ppm: 5.01, 5.05 (2 s, 2H, N-CH$_2$), 7.06 (t, 1H, Ar-H, J = 8.0 Hz), 7.17 (t, 1H, Ar-H, J = 8.0 Hz), 7.29– 7.32 (m, 4H, Ar-H), 7.42–7.48 (m, 2H, Ar-H), 7.69–7.73 (m, 1.5H, Ar-H), 7.77 (t, 1H, Ar-H, J = 8.0 Hz), 7.87, 8.02 (2 s, 1H, Ar-H), 8.09–8.12 (m, 1.5H, Ar-H), 12.01, 13.99 (2 s, 1H, NH); IR (KBr, ν cm^{-1}) 3309 (NH) and 1712, 1701 (2 C=O); MS m/z [%]: 476 [M$^+$+2, 16.41], 474 [M$^+$, 21.15], 475 [100]; Analysis calculated for $C_{24}H_{16}BrN_3O_3$: C, 60.77; H, 3.40; N, 8.86; found C, 60.98; H, 3.38; N, 8.75.

5.1.1.3.13. 5-Bromo-N′-(2-oxo-1-phenethylindolin-3-ylidene)benzofuran-2-carbohydrazide 7f.

Yellow powder (yield 78%), m.p. 239–241 °C; ^{1}H NMR ppm: 2.99 (br s, 2H, N-CH$_2$-CH$_2$), 4.03 (br s, 2H, N-CH$_2$-CH$_2$), 7.16–7.22 (m, 3H, Ar-H), 7.28–7.32 (m, 4H, Ar-H), 7.45 (t, 1H, Ar-H, J = 8.0 Hz), 7.46 (t, 2H, Ar-H, J = 8.0 Hz), 7.78 (d, 1H, Ar-H, J = 8.0 Hz), 7.85 (s, 1H, Ar-H), 8.09 (s, 1H, Ar-H), 11.97, 13.94 (2 s, 1H, NH); ^{13}C NMR δ ppm: 33.43 (N-CH$_2$-CH$_2$), 41.36 (N-CH$_2$-CH$_2$), 110.86, 114.71, 116.95, 119.34, 120.21, 121.53, 123.75, 126.15, 127.02, 127.92, 128.93, 129.34, 129.59, 130.55, 131.24, 132.58, 135.38, 138.58, 141.28, 143.61, 153.87, 161.36 (C=O indolin-2-one), 165.06 (C=O hydrazide); IR (KBr, ν cm^{-1}) 3356 (NH) and 1721, 1703 (2 C=O); Analysis calculated for C25H18BrN3O3: C, 61.49; H, 3.72; N, 8.60; found C, 61.63; H, 3.70; N, 8.66.

5.1.1.3.14. 5-Bromo-N′-(5-bromo-1-isobutyl-2-oxoindolin-3-ylidene)-benzofuran-2-carbohydrazide 7 g.

Orange powder (yield 74%), m.p. 244–246 °C; ^{1}H NMR ppm: 0.94 (d, 6H, –CH–(CH$_3$)$_2$, J = 7.6 Hz), 2.11–2.17 (m, 1H, N-CH$_2$-CH), 3.51 (d, 2H, N-CH$_2$, J = 8.0 Hz), 6.94–7.12 (m, 1H, Ar-H), 7.70 (d, 1H, Ar-H, J = 8.0 Hz), 7.73–7.80 (m, 2H, Ar-H), 8.10–8.18 (m, 2H, Ar-H), 8.35 (s, 1H, Ar-H), 12.12, 13.98 (2 s, 1H, NH); IR (KBr, ν cm^{-1}) 3358 (NH) and 1724, 1700 (2 C=O); Analysis calculated for C21H17Br2N3O3: C, 48.58; H, 3.30; N, 8.09; found C, 48.73; H, 3.27; N, 8.14.

5.1.1.3.15. N′-(1-Benzyl-5-bromo-2-oxoindolin-3-ylidene)-5-bromobenzofuran-2-carbohydrazide 7 h.

Yellow powder (yield 81%), m.p. 236–237 °C; ^{1}H NMR ppm: 5.00, 5.04 (2 s, 2H, N-CH$_2$), 7.03 (d, 1H, Ar-H, J = 8.0 Hz), 7.29–7.32 (m, 1H, Ar-H), 7.35–7.39 (m, 2H, Ar-H), 7.42 (d, 2H, Ar-H, J = 8.0 Hz), 7.51–7.61 (m, 1H, Ar-H), 7.66–7.70 (m, 1H, Ar-H), 7.73–7.77 (m, 2H, Ar-H), 7.87, 8.13 (2 s, 1H, Ar-H), 8.07 (s, 1H, Ar-H), 12.19, 13.87 (2 s, 1H, NH); IR (KBr, ν cm^{-1}) 3335 (NH) and 1731, 1708 (2 C=O); Analysis calculated for $C_{24}H_{15}Br_2N_3O_3$: C, 52.11; H, 2.73; N, 7.60; found C, 51.86; H, 2.74; N, 7.69.

5.1.1.4. Synthesis of 5-bromo-2-isocyanatobenzofuran 11.

5-Bromobenzofuran-2-carbonyl chloride 9 (1 g, 3.8 mmol) was dissolved in dry acetone (30 ml), then added drop wisely to aqueous solution of equivalent amount of NaN$_3$ at 0 °C over 30 min. The formed precipitate was filtrated under vacuum and washed with pet. ether, then heated without purification in dry toluene for 1 h to produce the intermediate 11.

5.1.1.5. Synthesis of hydrazones 12a-b.

To hot stirred solution of the appropriate indolin-2-one 6c and 6e (6 mmol) in isopropyl alcohol (22 ml), hydrazine hydrate (0.50 ml, 15 mmol) was added. The reaction solution was heated under reflux for 3 h, then cold to room temperature. The formed solid was collected via filtration, washed with n-hexane and recrystallized from acetonitrile to afford the key intermediates hydrazones 12a-b in a good yield (87–92%).

5.1.1.5.1. 3-Hydrazono-1-isobutylindolin-2-one 12a.

Yellow powder (yield 65%), m.p. 91–93 °C; ^{1}H NMR ppm: 0.98 (d, 6H, -CH-(CH$_3$)$_2$, J = 6.8 Hz), 2.02–2.12 (m, 1H, N-CH$_2$-CH), 3.55 (d, 2H, N-CH$_2$, J = 7.6 Hz), 7.02 (t, 1H, Ar-H, J = 7.6 Hz), 7.08 (d, 1H, Ar-H, J = 8.0 Hz), 7.21 (t, 1H, Ar-H, J = 8.0 Hz), 7.41 (d, 1H, Ar-H, J = 7.6 Hz), 9.67 (d, 1H, NH$_2$, D$_2$O exchangeable, J = 14.8 Hz), 10.54 (d, 1H, NH$_2$, D$_2$O exchangeable, J = 14.8 Hz); ^{13}C NMR δ ppm: 20.45 (–CH–(CH$_3$)$_2$), 27.39 (N–CH$_2$–CH), 46.40 (N–CH$_2$), 109.59, 117.73, 121.83, 122.23, 125.66, 127.45, 140.07, 161.49 (C=O indolin-2-one); Analysis calculated for $C_{12}H_{15}N_3O$: C, 66.34; H, 6.96; N, 19.34; found C, 66.53; H, 6.91; N, 19.39.

5.1.1.6. Synthesis of target compounds 13a-b.

To the previously prepared solution of isocyanate 11, equimolar amount of hydrazone 12a–b was added. The reaction mixture was heated for 4 h, the formed precipitate was filtrated while hot, washed with diethyl ether and recrystallized from DMF/EtOH mixture to produce targeted compounds 13a–b, respectively.

5.1.1.6.1. N-(5-Bromobenzofuran-2-yl)-2–(1-isobutyl-2-oxoindolin-3-ylidene)hydrazine-1-carboxamide 13a.

Yellow powder (yield 73%), m.p. 208–210 °C; ^{1}H NMR ppm: 0.94 (d, 6H, –CH–(CH$_3$)$_2$, J = 8.0 Hz), 2.06–2.13 (m, 1H, N–CH$_2$–CH), 3.57 (d, 2H, N-CH$_2$, J = 7.6 Hz), 6.55 (s, 1H, Ar-H), 6.63 (s, 0.5H, Ar-H), 7.15–7.21 (m, 1H, Ar-H), 7.28–7.32 (m, 1.5H, Ar-H), 7.41–7.47 (m, 2H, Ar-H), 7.70–7.74 (m, 2H, Ar-H), 10.12 (s, 1H, NH urea), 11.33 (s, 1H, NH urea); ^{13}C NMR δ ppm: 20.44 (–CH–(CH$_3$)$_2$), 27.28 (N–CH$_2$–CH), 66.82 (N–CH$_2$), 110.60, 112.52, 116.02, 119.90, 121.04, 122.52, 123.30, 125.07, 131.39, 132.27, 133.49, 143.34, 148.57, 148.99, 150.31, 151.01, 161.27 (C=O indolin-2-one), 165.09 (C=O hydrazide); IR (KBr, ν cm^{-1}) 3345, 3240 (2NH) and 1730, 1711 (2 C=O); MS m/z [%]: 457 [M$^+$+2, 27.45], 455 [M$^+$, 29.72], 414 [100]; Analysis calculated for $C_{21}H_{19}BrN_4O_3$: C, 55.40; H, 4.21; N, 12.31; found C, 55.59; H, 4.16; N, 12.42.

5.1.1.6.2. 2–(1-Benzyl-2-oxoindolin-3-ylidene)-N-(5-bromobenzofuran-2-yl)hydrazine-1-carboxamide 13 b.

Yellow powder (yield 68%), m.p. 217–219 °C; ^{1}H NMR ppm: 4.98 (s, 2H, N-CH$_2$), 6.53 (s, 1H, Ar-H), 6.61 (s, 1H, Ar-H), 7.02 (d, 1H, Ar-H, J = 8.0 Hz), 7.11 (t, 1H, Ar-H, J = 8.0 Hz), 7.25–7.30 (m, 2H, Ar-H), 7.31–7.38 (m, 3H, Ar-H), 7.41–7.45 (m, 2H, Ar-H), 7.68–7.71 (m, 2H, Ar-H), 10.10 (s, 1H, NH urea), 11.38 (s, 1H, NH urea); ^{13}C NMR δ ppm: 42.51 (CH$_2$), 115.57, 119.67, 120.62, 122.17, 123.04, 124.56, 124.73, 127.43, 127.63, 128.74, 130.81, 131.68, 132.92, 135.84, 142.18, 148.06, 148.21, 148.48, 149.75, 150.56, 150.69, 160.57 (C=O indolin-2-one), 165.06

(C＝O hydrazide); IR (KBr, ν cm^{-1}) 3334, 3270 (2NH) and 1728, 1707 (2 C＝O); Analysis calculated for $C_{24}H_{17}BrN_4O_3$: C, 58.91; H, 3.50; N, 11.45; found C, 59.22; H, 3.53; N, 11.52.

5.2. Biological evaluations

All experimental procedures utilised in the biological assays herein conducted were performed as reported earlier; anti-proliferation[115], cell cycle[116–117], Annexin V-FITC Apoptosis[118] and CDK2 kinase[119] assays, and have been provided in the Supplementary Materials.

5.3. Molecular docking study

All the molecular modelling simulations were performed using Molecular Operating Environment (MOE, 2010.10) software. All minimizations were carried out with MOE until an RMSD gradient of 0.05 kcal·mol^{-1}Å^{-1} with MMFF94× force field and the partial charges were automatically calculated. The X-ray crystallographic structure of CDK2 co-crystallized with an oxindole derivative (IC$_{50}$ = 60 nM) as inhibitor (PDB ID: 1FVT)[109] and of GSK-3β co-crystallized with the oxindole derivative Indirubin-3′-monoxime (IC$_{50}$ = 22 nM) as inhibitor (PDB ID: 1Q41)[110] were downloaded from the protein data bank[120]. The selection of these two protein structures specifically attributed to their co-crystallization with potent CDK2 and GSK-3β oxindole-based inhibitors, respectively.

For the CDK2 protein structure (PDB ID: 1FVT); water molecules were first removed, as for the GSK-3β protein structure (PDB ID: 1Q41); Chain B and water molecules which are not involved in binding were first removed, whereas, two conservative water molecules near chain A Thr138 that serve a functional role in the co-crystalized inhibitor binding were kept[110]. Then, the proteins were prepared for the docking study using *LigX* protocol in MOE with default options. The co-crystalized ligands were used to define the active site for docking. Triangle Matcher placement method and London dG scoring function were used for docking. Self-docking of the co-crystallized ligands in the active site of the kinase domains was first performed to validate the used docking protocol giving a docking pose with an energy score (S) = −10.63 kcal/mol and an RMSD of 0.894 Å in CDK2 (PDB ID: 1FVT) and energy score (S) = −12.00 kcal/mol and an RMSD of 0.471 Å in GSK-3β (PDB ID: 1Q41), Figure 7 and Table 5.

The validated docking protocols were then used to study the ligand-protein interactions of the newly synthesised compounds in the active site of the target kinases to predict their binding mode and establish their structure activity relationship (SAR) to rationalise their binding affinity.

Disclosure statement

No potential conflict of interest was reported by the author(s).

Funding

References

1. Manning G, Whyte DB, Martinez R, et al. The protein kinase complement of the human genome. Science 2002;298: 1912–34.
2. Parang K, Sun G. Protein kinase inhibitors drug discovery. In: Gad SC, ed. Drug discovery handbook. Hoboken, New Jersey: John Wiley & Sons, Inc; 2005:1191–1257.
3. Roskoski R. Jr. Classification of small molecule protein kinase inhibitors based upon the structures of their drug-enzyme complexes. Pharmacol Res 2016;103:26–48.
4. Allam HA, Aly EE, Farouk A, et al. Design and synthesis of some new 2,4,6-trisubstituted quinazoline EGFR inhibitors as targeted anticancer agents. Bioorg Chem 2020;98: 103726.
5. Al-Sanea MM, Elkamhawy A, Paik S, et al. Sulfonamide-based 4-anilinoquinoline derivatives as novel dual Aurora kinase (AURKA/B) inhibitors: synthesis, biological evaluation and in silico insights. Bioorg Med Chem 2020;28:115525.
6. Alonso A, Sasin J, Bottini N, et al. Protein tyrosine phosphatases in the human genome. Cell 2004;117:699–711.
7. Bononi A, Agnoletto C, De Marchi E, et al. Protein kinases and phosphatases in the control of cell fate. Enzyme Res 2011;2011:329098.
8. Zhang J, Yang PL, Gray NS. Targeting cancer with small molecule kinase inhibitors. Nat Rev Cancer 2009;9:28–39.
9. Fabbro D, Ruetz S, Buchdunger E, et al. Protein kinases as targets for anticancer agents: from inhibitors to useful drugs. Pharmacol Ther 2002;93:79–98.
10. Pearson M, García-Echeverría C, Fabbro D, Protein tyrosine kinases as targets for cancer and other indications. In: Fabbro D, Mc Cormick F, eds. Protein tyrosine kinases - from inhibitors to useful drugs. Totowa (NJ): Humana Press Inc.; 2006:1–29.
11. Sedlacek HH. Kinase inhibitors in cancer therapy: a look ahead. Drugs 2000;59:435–76.
12. Weinstein IB, Joe AK. Mechanisms of disease: oncogene addiction-a rationale for molecular targeting in cancer therapy. Nat Clin Pract Oncol 2006;3:448–57.
13. Padma VV. An overview of targeted cancer therapy. BioMedicine 2015;5:19.
14. Aggarwal S. Targeted cancer therapies. Nat Rev Drug Discov 2010;9:427–8.
15. Topcul M, Cetin I. Endpoint of cancer treatment: targeted therapies. Asian Pac J Cancer Prev 2014;15:4395–403.
16. Bray F, Ferlay J, Soerjomataram I, et al. Global cancer statistics 2018: GLOBOCAN estimates of incidence and mortality worldwide for 36 cancers in 185 countries. CA Cancer J Clin 2018;68:394–424.
17. American Cancer Society. Cancer Facts & Figures 2019. Available from: https://www.cancer.org/content/dam/cancer-org/research/cancer-facts-and-statistics/annual-cancer-facts-and-figures/2019/cancer-facts-and-figures-2019.pdf.
18. Yan JD, Liu Y, Zhang ZY, et al. Expression and prognostic significance of VEGFR-2 in breast cancer. Pathol Res Pract 2015;211:539–43.
19. Guo S, Colbert LS, Fuller M, et al. Vascular endothelial growth factor receptor-2 in breast cancer. Biochim Biophys Acta 2010;1806:108–21.
20. Abdel-Mohsen HT, Abd El-Meguid EA, El Kerdawy AM, et al. Design, synthesis, and molecular docking of novel 2-aryl-benzothiazole multiangiokinase inhibitors targeting breast cancer. Arch Pharm (Weinheim) 2020;353:e1900340.

21. Elbauomy Elsheikh S, Green AR, Lambros MBK, et al. FGFR1 amplification in breast carcinomas: a chromogenic in situ hybridisation analysis. Breast Cancer Research 2007;9:R23.

22. Vrekoussis T, Stathopoulos EN, Kafousi M, et al. Expression of endothelial PDGF receptors alpha and beta in breast cancer: up-regulation of endothelial PDGF receptor beta. Oncol Rep 2007;17:1115–9.

23. He X, Xiang H, Zong X, et al. CDK2-AP1 inhibits growth of breast cancer cells by regulating cell cycle and increasing docetaxel sensitivity in vivo and in vitro. Cancer Cell Int 2014;14:130.

24. Alexander A, Karakas C, Chen X, et al. Cyclin E overexpression as a biomarker for combination treatment strategies in inflammatory breast cancer. Oncotarget 2017;8: 14897–911.

25. Ding L, Cao J, Lin W, et al. The roles of cyclin-dependent kinases in cell-cycle progression and therapeutic strategies in human breast cancer. Int J Mol Sci 2020;21:1960.

26. Harwell RM, Porter DC, Danes C, Keyomarsi K. Processing of cyclin E differs between normal and tumor breast cells. Cancer Res 2000;60:481–9.

27. Cooley A, Zelivianski S, Jeruss JS. Impact of cyclin E overexpression on Smad3 activity in breast cancer cell lines. Cell Cycle 2010;9:4900–7.

28. Quintayo MA, Munro AF, Thomas J, et al. GSK3β and cyclin D1 expression predicts outcome in early breast cancer patients. Breast Cancer Res Treat 2012;136:161–8.

29. Walz A, Ugolkov A, Chandra S, et al. Molecular pathways: revisiting glycogen synthase Kinase-3β as a target for the treatment of cancer. Clin Cancer Res 2017;23:1891–7.

30. Duda P, Akula SM, Abrams SL, et al. Targeting GSK3 and associated signaling pathways involved in cancer. Cells 2020;9:1110.

31. Malumbres M. Physiological relevance of cell cycle kinases. Physiol Rev 2011;91:973–1007.

32. Malumbres M, Barbacid M. Mammalian cyclin-dependent kinases. Trends Biochem Sci 2005;30: 630–41.

33. Lapenna S, Giordano A. Cell cycle kinases as therapeutic targets for cancer. Nat Rev Drug Discov 2009;8:547–66.

34. Luk KC, Simcox ME, Schutt A, et al. A new series of potent oxindole inhibitors of CDK2. Bioorg Med Chem Lett 2004; 14:913–7.

35. Chohan TA, Qayyum A, Rehman K, et al. An insight into the emerging role of cyclin-dependent kinase inhibitors as potential therapeutic agents for the treatment of advanced cancers. Biomed Pharmacother 2018;107:1326–41.

36. Chohan TA, Qian H, Pan Y, Chen JZ. Cyclin-dependent kinase-2 as a target for cancer therapy: progress in the development of CDK2 inhibitors as anti-cancer agents. Curr Med Chem 2015;22:237–63.

37. Abd El-Karim SS, Syam YM, El Kerdawy AM, Abdelghany TM. New thiazol-hydrazono-coumarin hybrids targeting human cervical cancer cells: synthesis, CDK2 inhibition, QSAR and molecular docking studies. Bioorg Chem 2019; 86:80–96.

38. Horiuchi D, Huskey NE, Kusdra L, et al. Chemical-genetic analysis of cyclin dependent kinase 2 function reveals an important role in cellular transformation by multiple oncogenic pathways. Proc Natl Acad Sci U S A 2012;109: E1019–27.

39. Ali S, Heathcote DA, Kroll SH, et al. The development of a selective cyclin-dependent kinase inhibitor that shows anti-tumor activity. Cancer Res 2009;69:6208–15.

40. Węsierska-Gądek J, Gritsch D, Zulehner N, et al. Roscovitine, a selective CDK inhibitor, reduces the basal and estrogen-induced phosphorylation of ER-α in human ER-positive breast cancer cells. J Cell Biochem 2011;112: 761–72.

41. Johnson N, Bentley J, Wang LZ, et al. Pre-clinical evaluation of cyclin-dependent kinase 2 and 1 inhibition in anti-estrogen-sensitive and resistant breast cancer cells. Br J Cancer 2010;102:342–50.

42. Welsh GI, Proud CG. Glycogen synthase kinase-3 is rapidly inactivated in response to insulin and phosphorylates eukaryotic initiation factor eIF-2B. Biochem J 1993;294: 625–9.

43. Frame S, Cohen P, Biondi RM. A common phosphate binding site explains the unique substrate specificity of GSK3 and its inactivation by phosphorylation. Mol Cell 2001;7: 1321–7.

44. Hooper C, Killick R, Lovestone S. The GSK3 hypothesis of Alzheimer's disease. J Neurochem 2008;104:1433–9.

45. Bhat RV, Budd Haeberlein SL, Avila J. Glycogen synthase kinase 3: a drug target for CNS therapies. J Neurochem 2004;89:1313–7.

46. Hughes K, Nikolakaki E, Plyte SE, et al. Modulation of the glycogen synthase kinase-3 family by tyrosine phosphorylation. Embo J 1993;12:803–8.

47. Martinez A, Castro A, Dorronsoro I, Alonso M. Glycogen synthase kinase 3 (GSK-3) inhibitors as new promising drugs for diabetes, neurodegeneration, cancer, and inflammation. Med Res Rev 2002;22:373–84.

48. Avila J, Leon-Espinosa G, Garcia E, et al. Tau phosphorylation by GSK3 in different conditions. Int J Alzheimers Dis 2012;2012:578373.

49. Doble BW, Woodgett JR. GSK-3: tricks of the trade for a multi-tasking kinase. J Cell Sci 2003;116:1175–86.

50. El Kerdawy AM, Osman AA, Zaater MA. Receptor-based pharmacophore modeling, virtual screening, and molecular docking studies for the discovery of novel GSK-3β inhibitors. J Mol Model 2019;25:171.

51. Gaisina IN, Gallier F, Ougolkov AV, et al. From a natural product lead to the identification of potent and selective benzofuran-3-yl-(indol-3-yl)maleimides as glycogen synthase kinase 3beta inhibitors that suppress proliferation and survival of pancreatic cancer cells. J Med Chem 2009; 52:1853–63.

52. Ugolkov A, Gaisina I, Zhang JS, et al. GSK-3 inhibition overcomes chemoresistance in human breast cancer. Cancer Lett 2016;380:384–92.

53. Branca MA. Multi-kinase inhibitors create buzz at ASCO. Nat Biotechnol 2005;23:639.

54. Broekman F, Giovannetti E, Peters GJ. Tyrosine kinase inhibitors: multi-targeted or single-targeted? World J Clin Oncol 2011;2:80–93.

55. Krug M, Hilgeroth A. Recent advances in the development of multi-kinase inhibitors. Mini Rev Med Chem 2008;8: 1312–27.

56. Muller-Tidow C, Diederichs S, Bulk E, et al. Identification of metastasis-associated receptor tyrosine kinases in non-small cell lung cancer. Cancer Res 2005;65:1778–82.

57. Garuti L, Roberti M, Bottegoni G. Multi-kinase inhibitors. Curr Med Chem 2015;22:695–712.

58. Abdel-Mohsen HT, Omar MA, El Kerdawy AM, et al. Novel potent substituted 4-amino-2-thiopyrimidines as dual

VEGFR-2 and BRAF kinase inhibitors. Eur J Med Chem 2019;179:707–22.

59. Lozinskaya NA, Babkov DA, Zaryanova EV, et al. Synthesis and biological evaluation of 3-substituted 2-oxindole derivatives as new glycogen synthase kinase 3β inhibitors. Bioorg Med Chem 2019;27:1804–17.

60. Ouach A, Boulahjar R, Vala C, et al. Novel optimization of valmerins (tetrahydropyrido[1,2-a]isoindolones) as potent dual CDK5/GSK3 inhibitors. Eur J Med Chem 2016;115: 311–25.

61. Xu M, Wang SL, Zhu L, et al. Structure-activity relationship (SAR) studies of synthetic glycogen synthase kinase-3β inhibitors: a critical review. Eur J Med Chem 2019;164: 448–70.

62. Boulahjar R, Ouach A, Bourg S, et al. Advances in tetrahydropyrido[1,2-a]isoindolone (valmerins) series: potent glycogen synthase kinase 3 and cyclin dependent kinase 5 inhibitors. Eur J Med Chem 2015;101:274–87.

63. Boulahjar R, Ouach A, Matteo C, et al. Novel tetrahydropyrido[1,2-a]isoindolone derivatives (valmerins): potent cyclin-dependent kinase/glycogen synthase kinase 3 inhibitors with antiproliferative activities and antitumor effects in human tumor xenografts. J Med Chem 2012;55:9589–606.

64. Polychronopoulos P, Magiatis P, Skaltsounis AL, et al. Structural basis for the synthesis of indirubins as potent and selective inhibitors of glycogen synthase kinase-3 and cyclin-dependent kinases. J Med Chem 2004;47:935–46.

65. Mettey Y, Gompel M, Thomas V, et al. Aloisines, a new family of CDK/GSK-3 inhibitors. SAR study, crystal structure in complex with CDK2, enzyme selectivity, and cellular effects. J Med Chem 2003;46:222–36.

66. Zhao P, Li Y, Gao G, et al. Design, synthesis and biological evaluation of N-alkyl or aryl substituted isoindigo derivatives as potential dual cyclin-dependent kinase 2 (CDK2)/glycogen synthase kinase 3β (GSK-3β) phosphorylation inhibitors. Eur J Med Chem 2014;86:165–74.

67. Patel DS, Dessalew N, Iqbal P, Bharatam PV. Structure-based approaches in the design of GSK-3 selective inhibitors. Curr Protein Pept Sci 2007;8:352–64.

68. Arfeen M, Patel R, Khan T, Bharatam PV. Molecular dynamics simulation studies of GSK-3β ATP competitive inhibitors: understanding the factors contributing to selectivity. J Biomol Struct Dyn 2015;33:2578–93.

69. Echalier A, Endicott JA, Noble ME. Recent developments in cyclin-dependent kinase biochemical and structural studies. Biochim Biophys Acta 2010;1804:511–9.

70. Davies TG, Tunnah P, Meijer L, et al. Inhibitor binding to active and inactive CDK2: the crystal structure of CDK2-cyclin A/indirubin-5-sulphonate. Structure 2001;9:389–97.

71. Czelen P. Inhibition mechanism of CDK-2 and GSK-3beta by a sulfamoylphenyl derivative of indoline-a molecular dynamics study. J Mol Model 2017;23:230.

72. Pacureanu L, Avram S, Bora A, et al. Portraying the selectivity of GSK-3 inhibitors towards CDK-2 by 3D similarity and molecular docking. Struct Chem 2019;30:911–23.

73. Ko HW, Kim EY, Chiu J, et al. A hierarchical phosphorylation cascade that regulates the timing of PERIOD nuclear entry reveals novel roles for proline-directed kinases and GSK-3beta/SGG in circadian clocks. J Neurosci 2010;30: 12664–75.

74. Leclerc S, Garnier M, Hoessel R, et al. Indirubins inhibit glycogen synthase kinase-3 beta and CDK5/p25, two protein kinases involved in abnormal tau phosphorylation in Alzheimer's disease. A property common to most cyclin-dependent kinase inhibitors? J Biol Chem 2001;276:251–60.

75. Bhat R, Xue Y, Berg S, et al. Structural insights and biological effects of glycogen synthase kinase 3-specific inhibitor AR-A014418. J Biol Chem 2003;278:45937–45.

76. Vine KL, Matesic L, Locke JM, et al. Cytotoxic and anticancer activities of isatin and its derivatives: a comprehensive review from 2000–2008. Anticancer Agents Med Chem 2009;9:397–414.

77. Abdel-Aziz HA, Eldehna WM, Keeton AB, et al. Isatin-benzoazine molecular hybrids as potential antiproliferative agents: synthesis and in vitro pharmacological profiling. Drug Des Devel Ther 2017;11:2333–46.

78. Al-Warhi T, El Kerdawy AM, Aljaeed N, et al. Synthesis, biological evaluation and in silico studies of certain oxindole-indole conjugates as anticancer CDK inhibitors. Molecules 2020;25:2031.

79. Goodman VL, Rock EP, Dagher R, et al. Approval summary: sunitinib for the treatment of imatinib refractory or intolerant gastrointestinal stromal tumors and advanced renal cell carcinoma. Clin Cancer Res 2007;13:1367–73.

80. Inomata M, Nishioka Y, Azuma A. Nintedanib: evidence for its therapeutic potential in idiopathic pulmonary fibrosis. Core Evid 2015;10:89–98.

81. Jagtap AD, Chang PT, Liu JR, et al. Novel acylureidoindolin-2-one derivatives as dual Aurora B/FLT3 inhibitors for the treatment of acute myeloid leukemia. Eur J Med Chem 2014;85:268–88.

82. Yousefian M, Ghodsi R. Structure-activity relationship studies of indolin-2-one derivatives as vascular endothelial growth factor receptor inhibitors and anticancer agents. Arch Pharm (Weinheim) 2020;353:e2000022.

83. Eldehna WM, El Kerdawy AM, Al-Ansary GH, et al. Type IIA - Type IIB protein tyrosine kinase inhibitors hybridization as an efficient approach for potent multikinase inhibitor development: design, synthesis, anti-proliferative activity, multikinase inhibitory activity and molecular modeling of novel indolinone-based ureides and amides. Eur J Med Chem 2019;163:37–53.

84. Laufer R, Forrest B, Li SW, et al. The discovery of PLK4 inhibitors: (E)-3-((1H-Indazol-6-yl)methylene)indolin-2-ones as novel antiproliferative agents. J Med Chem 2013;56: 6069–87.

85. Wang HC, Jagtap AD, Chang PT, et al. Bioisosteric replacement of an acylureido moiety attached to an indolin-2-one scaffold with a malonamido or a 2/4-pyridinoylamido moiety produces a selectively potent Aurora-B inhibitor. Eur J Med Chem 2014;84:312–34.

86. Zhong Y, Xue M, Zhao X, et al. Substituted indolin-2-ones as p90 ribosomal S6 protein kinase 2 (RSK2) inhibitors: molecular docking simulation and structure-activity relationship analysis. Bioorg Med Chem 2013;21:1724–34.

87. Aneja B, Khan NS, Khan P, et al. Design and development of Isatin-triazole hydrazones as potential inhibitors of microtubule affinity-regulating kinase 4 for the therapeutic management of cell proliferation and metastasis. Eur J Med Chem 2019;163:840–52.

88. Dweedar HE, Mahrous H, Ibrahim HS, Abdel-Aziz HA. Analogue-based design, synthesis and biological evaluation of 3-substituted-(methylenehydrazono)indolin-2-ones as anticancer agents. Eur J Med Chem 2014;78:275–80.

89. Hoessel R, Leclerc S, Endicott JA, et al. Indirubin, the active constituent of a Chinese antileukaemia medicine, inhibits cyclin-dependent kinases. Nat Cell Biol 1999;1:60–7.

90. Damiens E, Baratte B, Marie D, et al. Anti-mitotic properties of indirubin-3'-monoxime, a CDK/GSK-3 inhibitor: induction of endoreplication following prophase arrest. Oncogene 2001;20:3786–97.

91. Marko D, Schatzle S, Friedel A, et al. Inhibition of cyclin-dependent kinase 1 (CDK1) by indirubin derivatives in human tumour cells. Br J Cancer 2001;84:283–9.

92. Liang C, Xia J, Lei D, et al. Synthesis, in vitro and in vivo antitumor activity of symmetrical bis-Schiff base derivatives of isatin. Eur J Med Chem 2014;74:742–50.

93. Meijer L, Skaltsounis AL, Magiatis P, et al. GSK-3-selective inhibitors derived from Tyrian purple indirubins. Chem Biol 2003;10:1255–66.

94. Khanam H, Shamsuzzaman , Bioactive Benzofuran derivatives: a review. Eur J Med Chem 2015;97:483–504.

95. Miao Y-h, Hu Y-h, Yang J, et al. Natural source, bioactivity and synthesis of benzofuran derivatives. RSC Adv 2019;9:27510–40.

96. Hassan GS, Georgey HH, George RF, Mohamed ER. Aurones and furoaurones: biological activities and synthesis. Bull Faculty Pharm Cairo Univ 2018;56:121–7.

97. Eldehna WM, Nocentini A, Elsayed ZM, et al. Benzofuran-based carboxylic acids as carbonic anhydrase inhibitors and antiproliferative agents against breast cancer. ACS Med Chem Lett 2020;11:1022–7.

98. Xiang Y, Hirth B, Asmussen G, et al. The discovery of novel benzofuran-2-carboxylic acids as potent Pim-1 inhibitors. Bioorg Med Chem Lett 2011;21:3050–6.

99. Salomé C, Narbonne V, Ribeiro N, et al. Benzofuran derivatives as a novel class of inhibitors of mTOR signaling. Eur J Med Chem 2014;74:41–9.

100. Salomé C, Ribeiro N, Chavagnan T, et al. Benzofuran derivatives as anticancer inhibitors of mTOR signaling. Eur J Med Chem 2014;81:181–91.

101. Abd El-Karim SS, Anwar MM, Mohamed NA, et al. Design, synthesis, biological evaluation and molecular docking studies of novel benzofuran-pyrazole derivatives as anticancer agents. Bioorg Chem 2015;63:1–12.

102. Mosmann T. Rapid colorimetric assay for cellular growth and survival: Application to proliferation and cytotoxicity assays. J Immunol Methods 1983;65:55–63.

103. Cherukupalli S, Chandrasekaran B, Krystof V, et al. Synthesis, anticancer evaluation, and molecular docking studies of some novel 4,6-disubstituted pyrazolo[3,4-d]pyrimidines as cyclin-dependent kinase 2 (CDK2) inhibitors. Bioorg Chem 2018;79:46–59.

104. Oakes V, Wang W, Harrington B, et al. Cyclin A/Cdk2 regulates Cdh1 and claspin during late S/G2 phase of the cell cycle. Cell Cycle 2014;13:3302–11.

105. Martin A, Odajima J, Hunt SL, et al. Cdk2 is dispensable for cell cycle inhibition and tumor suppression mediated by p27(Kip1) and p21(Cip1). Cancer Cell 2005;7:591–8.

106. Acikgoz E, Guler G, Camlar M, et al. Glycogen synthase kinase-3 inhibition in glioblastoma multiforme cells induces apoptosis, cell cycle arrest and changing biomolecular structure. Spectrochim Acta A Mol Biomol Spectrosc 2019;209:150–64.

107. Rashid MS, Mazur T, Ji W, et al. Analysis of the role of GSK3 in the mitotic checkpoint. Sci Rep 2018;8:14259.

108. Gorczyca W. Cytometric analyses to distinguish death processes. Endocr Relat Cancer 1999;6:17–9.

109. Davis ST, Benson BG, Bramson HN, et al. Prevention of chemotherapy-induced alopecia in rats by CDK inhibitors. Science 2001;291:134–7.

110. Bertrand JA, Thieffine S, Vulpetti A, et al. Structural characterization of the GSK-3beta active site using selective and non-selective ATP-mimetic inhibitors. J Mol Biol 2003;333:393–407.

111. Attia MI, Eldehna WM, Afifi SA, et al. New hydrazonoindolin-2-ones: Synthesis, exploration of the possible anti-proliferative mechanism of action and encapsulation into PLGA microspheres. Plos One 2017;12:e0181241.

112. Abo-Ashour MF, Eldehna WM, Nocentini A, et al. Novel hydrazido benzenesulfonamides-isatin conjugates: synthesis, carbonic anhydrase inhibitory activity and molecular modeling studies. Eur J Med Chem 2018;157:28–36.

113. Lee J, Khanapure SP, Kim H-O, et al. Efficient synthesis of a benzo[b]furan building block. Synth Commun 2010;40:3390–6.

114. Eldehna WM, Abo-Ashour MF, Ibrahim HS, et al. Novel [(3-indolylmethylene)hydrazono]indolin-2-ones as apoptotic anti-proliferative agents: design, synthesis and in vitro biological evaluation. J Enzyme Inhibit Med Chem 2018;33:686–700.

115. Sabt A, Abdelhafez OM, El-Haggar RS, et al. Novel coumarin-6-sulfonamides as apoptotic anti-proliferative agents: synthesis, in vitro biological evaluation, and QSAR studies. J Enzyme Inhibit Med Chem 2018;33:1095–107.

116. Mahdy HA, Ibrahim MK, Metwaly AM, et al. Design, synthesis, molecular modeling, in vivo studies and anticancer evaluation of quinazolin-4(3H)-one derivatives as potential VEGFR-2 inhibitors and apoptosis inducers. Bioorg Chem 2020;94:103422.

117. Eldehna WM, Hassan GS, Al-Rashood ST, et al. Synthesis and in vitro anticancer activity of certain novel 1-(2-methyl-6-arylpyridin-3-yl)-3-phenylureas as apoptosis-inducing agents. J Enzyme Inhibit Med Chem 2019;34:322–32.

118. Elmetwally SA, Saied KF, Eissa IH, Elkaeed EB. Design, synthesis and anticancer evaluation of thieno[2,3-d]pyrimidine derivatives as dual EGFR/HER2 inhibitors and apoptosis inducers. Bioorgan Chem 2019;88:102944.

119. Sabt A, Eldehna WM, Al-Warhi T, et al. Discovery of 3,6-disubstituted pyridazines as a novel class of anticancer agents targeting cyclin-dependent kinase 2: synthesis, biological evaluation and in silico insights. J Enzyme Inhibit Med Chem 2020;35:1616–30.

120. Protein Data Bank. https://www.rcsb.org/ [last accessed 10 Oct 2020].